NASA TechBriefs

National Aeronautics and
Space Administration


Electronic Components and Circuits


Electronic Systems


Physical Sciences


Materials


Computer Programs


Mechanics


Machinery


Fabrication Technology


Mathematics and Information Sciences


Life Sciences

00-01 January 2000

INTRODUCTION

Tech Briefs are short announcements of innovations originating from research and development activities of the National Aeronautics and Space Administration. They emphasize information considered likely to be transferable across industrial, regional, or disciplinary lines and are issued to encourage commercial application.

Availability of NASA Tech Briefs and TSPs

Requests for individual Tech Briefs or for Technical Support Packages (TSPs) announced herein should be addressed to

National Technology Transfer Center
Telephone No. (**800) 678-6882** or via World Wide Web at **www2.nttc.edu/leads/**

Please reference the control numbers appearing at the end of each Tech Brief. Information on NASA's Commercial Technology Team, its documents, and services is also available at the same facility or on the World Wide Web at **www.nctn.hq.nasa.gov**.

Commercial Technology Offices and Patent Counsels are located at NASA field centers to provide technology-transfer access to industrial users. Inquiries can be made by contacting NASA field centers and program offices listed below.

NASA Field Centers and Program Offices

Ames Research Center
Caroline Blake
(650) 604-0893 or
cblake@mail.arc.nasa.gov

Dryden Flight Research Center
Lee Duke
(805) 258-3802 or
lee.duke@dfrc.nasa.gov

Goddard Space Flight Center
George Alcorn
(301) 286-5810 or
galcorn@gsfc.nasa.gov

Jet Propulsion Laboratory
Merle McKenzie
(818) 354-2577 or
merle.mckenzie@cmail.jpl.nasa.gov

Johnson Space Center
Hank Davis
(281) 483-0474 or
hdavis@gp101.jsc.nasa.gov

John F. Kennedy Space Center
Gale Allen
(407) 867-6626 or
galeallen-1@ksc.nasa.gov

Langley Research Center
Dr. Joseph S. Heyman
(804) 864-6006 or
j.s.heyman@larc.nasa.gov

Glenn Research Center
Larry Viterna
(216) 433-3484 or
cto@lerc.nasa.gov

George C. Marshall Space Flight Center
Sally Little
(256) 544-4266 or
sally.little@msfc.nasa.gov

John C. Stennis Space Center
Kirk Sharp
(228) 688-1929 or
ksharp@ssc.nasa.gov

NASA Program Offices
At NASA Headquarters there are seven major program offices that develop and oversee technology projects of potential interest to industry:

Carl Ray
Small Business Innovation Research Program (SBIR) & Small Business Technology Transfer Program (STTR)
(202) 358-4652 or
cray@mail.hq.nasa.gov

Dr. Robert Norwood
Office of Aeronautics and Space Transportation Technology (Code R)
(202) 358-2320 or
rnorwood@mail.hq.nasa.gov

John Mulcahy
Office of Space Flight (Code MP)
(202) 358-1401 or
jmulcahy@mail.hq.nasa.gov

Gerald Johnson
Office of Aeronautics (Code R)
(202) 358-4711 or
g_johnson@aeromail.hq.nasa.gov

Bill Smith
Office of Space Science (Code S)
(202) 358-2473 or
wsmith@sm.ms.ossa.hq.nasa.gov

Roger Crouch
Office of Microgravity Science Applications (Code U)
(202) 358-0689 or
rcrouch@hq.nasa.gov

Granville Paules
Office of Mission to Planet Earth (Code Y)
(202) 358-0706 or
gpaules@mtpe.hq.nasa.gov

NASA TechBriefs

National Aeronautics and Space Administration

January 2000
00-01

Electronic Components and Circuits

Hardware, Techniques, and Processes

Books and Reports

Segmented-Cold-Cathode Display Panels

In comparison with CRTs, these panels could be much wider and thinner.

Goddard Space Flight Center, Greenbelt, Maryland

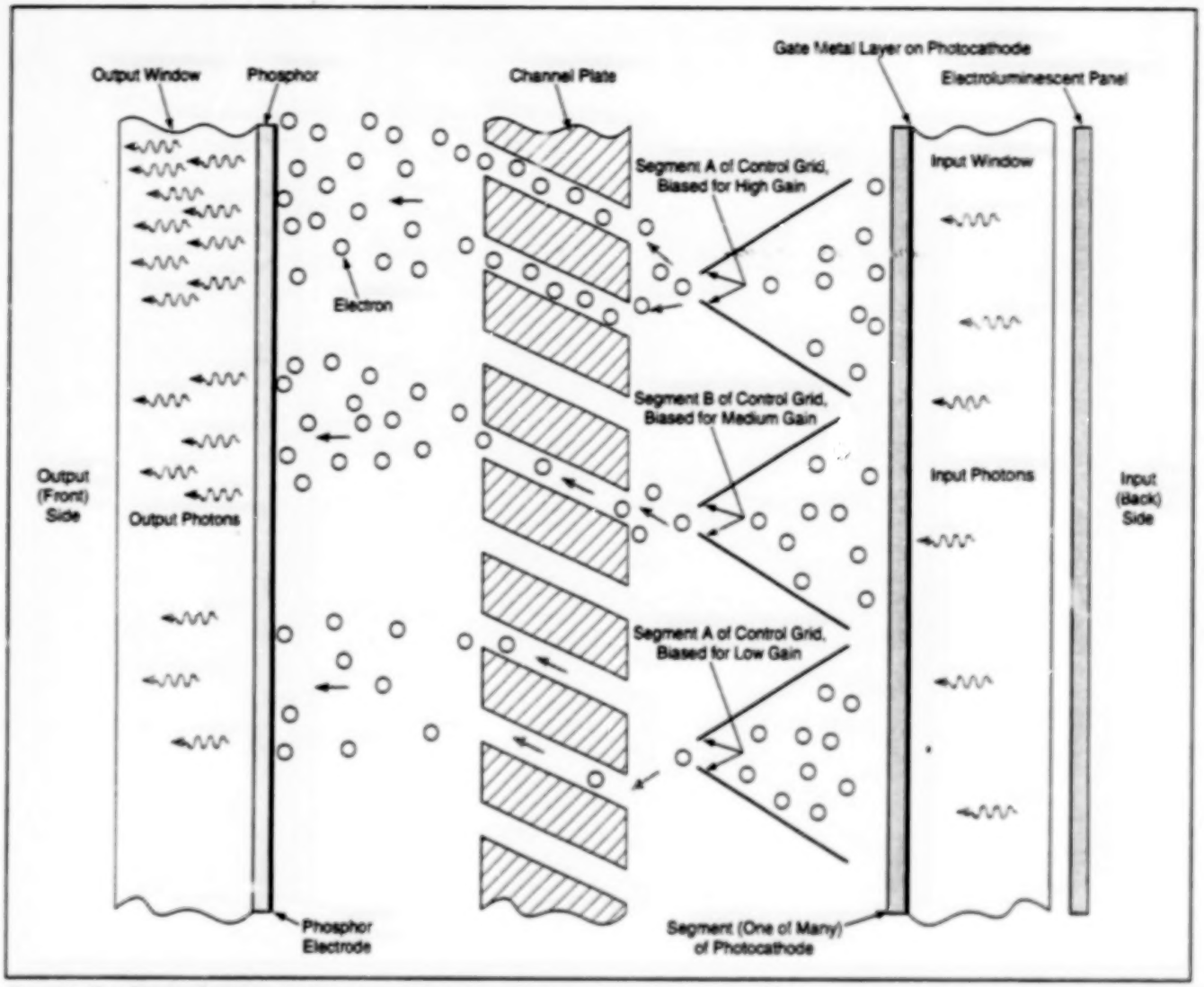

Figure 1. This **Display Panel** would include a proximity-focused channel-plate image intensifier with a segmented control grid and a segmented photocathode illuminated by an electroluminescent panel.

Display panels based largely on the principles of proximity-focused image-intensifier tubes have been proposed as alternatives to cathode-ray tubes (CRTs) and other conventional devices for wide displays. A panel of the proposed type would afford the high brightness and wide viewing angle (almost 180°) of a CRT, but it could readily be made much wider than the maximum dimension [50 in. (127 cm) diagonal] of currently available CRTs. The thickness of the panel [<4 in. (<10.2 cm)] would be much less than the depth of a typical CRT. Moreover, unlike a CRT, the panel would not introduce any geometric distortion into the displayed image because the image geometry would be established by a pixel structure within the panel.

Partly ignoring the two-dimensional aspect of the display for the moment, some basic physical aspects of the panel can be explained by reference to Figure 1. An electroluminescent panel on the back side would supply photons for excitation of a segmented photocathode. The photons would travel through an input window and through a transparent gate metal layer into the photocathode segment. The gate of the photocathode segment would be biased at about −20 V, relative to a channel plate, to encourage photoemission of electrons and force the emitted electrons toward the channel plate. A control grid based on the same principle as that of a control grid in a triode vacuum tube would be variably biased (probably to a potential between −10 and −30 V) to control the local brightness of the display by allowing more or fewer electrons to pass to the channel plate.

The channel plate would be about 2 cm thick, and the pores in the channel plate would be about 0.5 mm wide. The output side of the channel plate would be biased to a maximum potential of about 1 kV relative to the input side, so that the number of electrons striking the input pores of the channel plate would be multiplied to a large magnitude. The resulting cloud of electrons emerging from each pore in the channel plate would encounter an electric field that would accelerate the electrons toward a phosphor. The electric field would be provided by biasing a phosphor electrode at

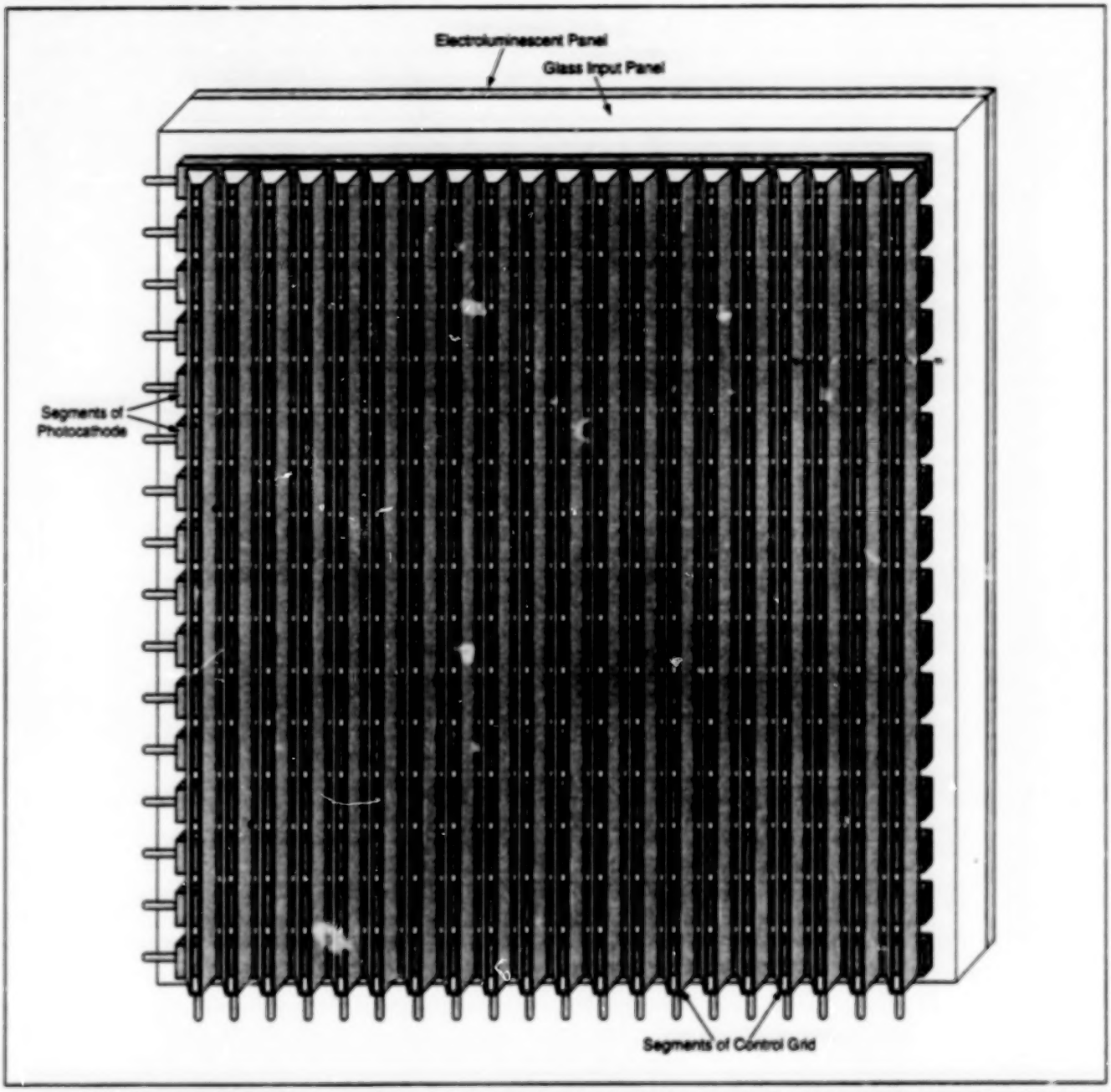

Figure 2. **Pixels Would Be Defined** by intersections of photocathode and control-grid segments. The photocathode segments would be activated sequentially to turn on rows of pixels sequentially. The brightness of each pixel in a row during its "on" period would be controlled via the voltage applied to the corresponding control-grid segment.

about 22 kV relative to the output side of the channel plate.

The phosphor electrode would be about 1,000 Å thick — thick enough to be opaque to light coming from behind but thin enough to pass electrons with kinetic energy >2 keV. Thus, the electrons would lose about 2 keV of kinetic energy traversing the phosphor electrode and would deposit the remainder of their kinetic energy in the phosphor, causing the phosphor to glow. The local intensity of the glow would depend on the bias applied to the local control grid. A multicolor display could be implemented by placing groups of red, green, and blue phosphors in registration with groups of three control grids in red/green/blue sequence. Thus, a multicolor display would contain three times the number of control grids of a monochrome display.

The two-dimensional aspect of the display can be explained by reference to Figure 2. A pixel would be defined by an intersection between one of the vertical control-grid segments and one of the horizontal photocathode segments. The minimum pixel size would be of the order of 1 mm; although this size is too large for the desired resolution in a small display that would ordinarily be implemented in a liquid-crystal display unit, it is an appropriate size for a wide-screen television or similar display. One of the advantages of larger pixels is greater ease of fabrication.

During operation, one photocathode segment (defining a row of pixels) would be biased to promote photoemission while the other photocathode segments would be biased to inhibit photoemission. During a frame period, rows of pixels would thus be turned on sequentially, the sequence repeating for each subsequent frame period. During the "on" period for each row, each control-grid segment would be

biased to the potential needed to obtain the desired brightness in the pixel lying at the intersection of the control-grid segment and the activated photocathode segment. An alternate version of this display panel replaces the channel plate with a uniform grid mesh. This mesh is biased to the same level as the channel-plate input side. Although this version of the display will not be as bright as the channel-plate version, existing photocathode materials support current densities that will allow output light levels near that of conventional CRTs without using a channel-plate electron multiplier. Also, this alternate version is substantially easier to fabricate.

This work was done by Leslie James Payne of **Goddard Space Flight Center**. *Further information is contained in a TSP [see page 1].*

This invention is owned by NASA, and a patent application has been filed. Inquiries concerning nonexclusive or exclusive license for its commercial development should be addressed to the Patent Counsel, Goddard Space Flight Center [see page 1]. Refer to GSC-13708.

Tunable HTS/Ferroelectric Microstrip Band-Pass Filters

These filters are designed for operation at temperatures less than about 77 K.

John H. Glenn Research Center, Cleveland, Ohio

Electrically tunable microstrip two-pole band-pass filters for a center frequency near 19 GHz and a 4-percent bandwidth have been designed, fabricated, and demonstrated to be functional. These filters are suitable for use in the front ends of K-band communication receivers that operate at low temperatures.

Figure 1 depicts the multilayer configuration and microstrip layout of one of these filters. The top layer is a thin film of the high-temperature superconductor (HTS) $YBa_2Cu_3O_{7-\delta}$ patterned into microstrip lines. The top layer rests on a layer of the ferroelectric material $SrTiO_3$, which rests on a dielectric layer of $LaAlO_3$. The bottom of the $LaAlO_3$ is coated with a thin film of a normal conductor (Au), which serves as a ground plane.

Tunability is achieved through the nonlinearity (specifically, the variation of permittivity with electric field) of the $SrTiO_3$ layer. Using a commercial electromagnetic-analysis computer-aided-engineering software package, the design of the filter was optimized so that normal operation at the center frequency would occur when the relative permittivity ε_r of the $SrTiO_3$ was 1,650. This resulted in a requirement to maintain a suitable bias in order to maintain ε_r at 1,650.

Prototypes of these filters were packaged for swept-frequency measurements of their scattering parameters (S_{ij}) in a helium-gas closed-cycle cryogenic system. In experiments on tunability, a dual-polarity biasing technique was used. Referring again to Figure 1, nodes A and C were biased with a positive voltage, while nodes B and D were biased with a negative voltage of equal magnitude. The dc bias connections at A and D were made via input and output bias tees; the bias connections at B and C were achieved via gold-wire bonds on radial biasing stubs. The dc bias was increased from 0 to ±500 V in steps of ±50 V.

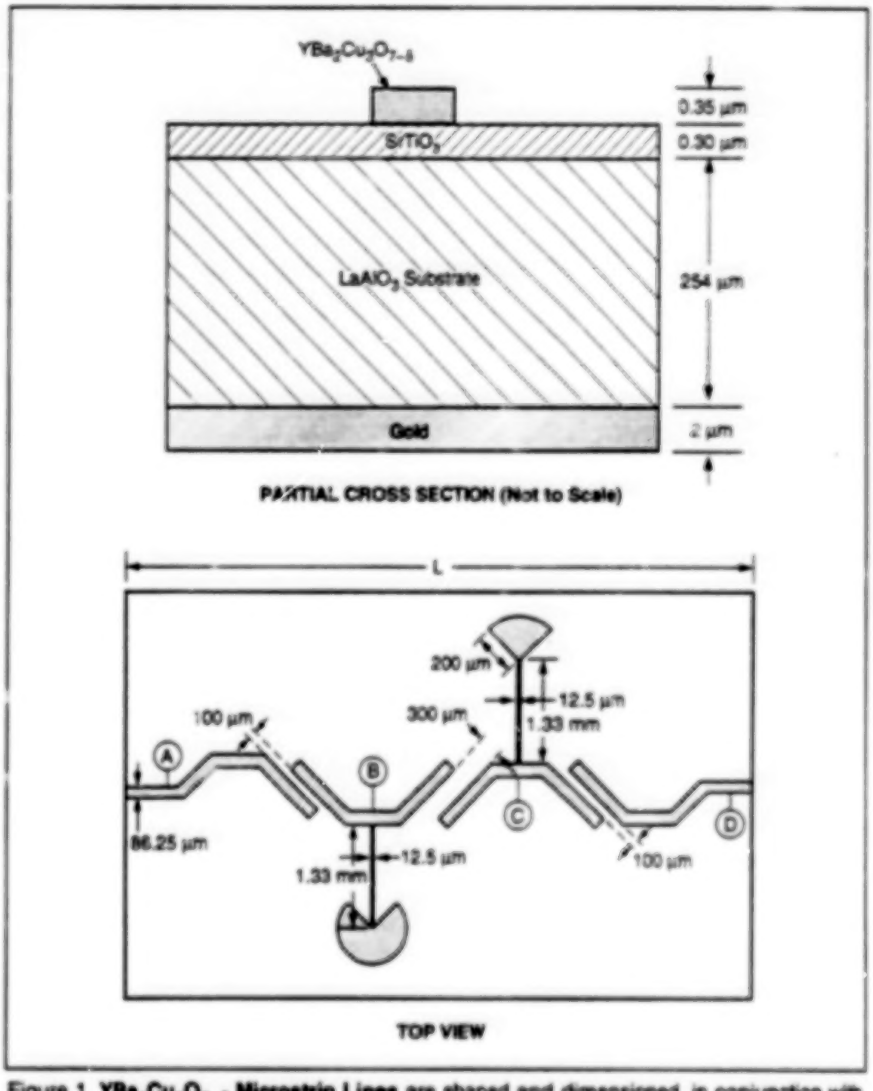

Figure 1. $YBa_2Cu_3O_{7-\delta}$ Microstrip Lines are shaped and dimensioned, in conjunction with the underlying layers, to obtain the desired two-pole pass-band frequency response. The pass band is adjusted by varying the dc bias and thus the electric field in the $SrTiO_3$ layer.

Figure 2 depicts results of some of the measurements; namely, the frequency and voltage dependence of S_{11} and S_{12} of one of the filters at a temperature of 77 K and an input power of 10 dBm. With increasing bias voltage, the center frequency of the filter shifted from 17.4 GHz at no bias to 19.1 GHz at a bias of

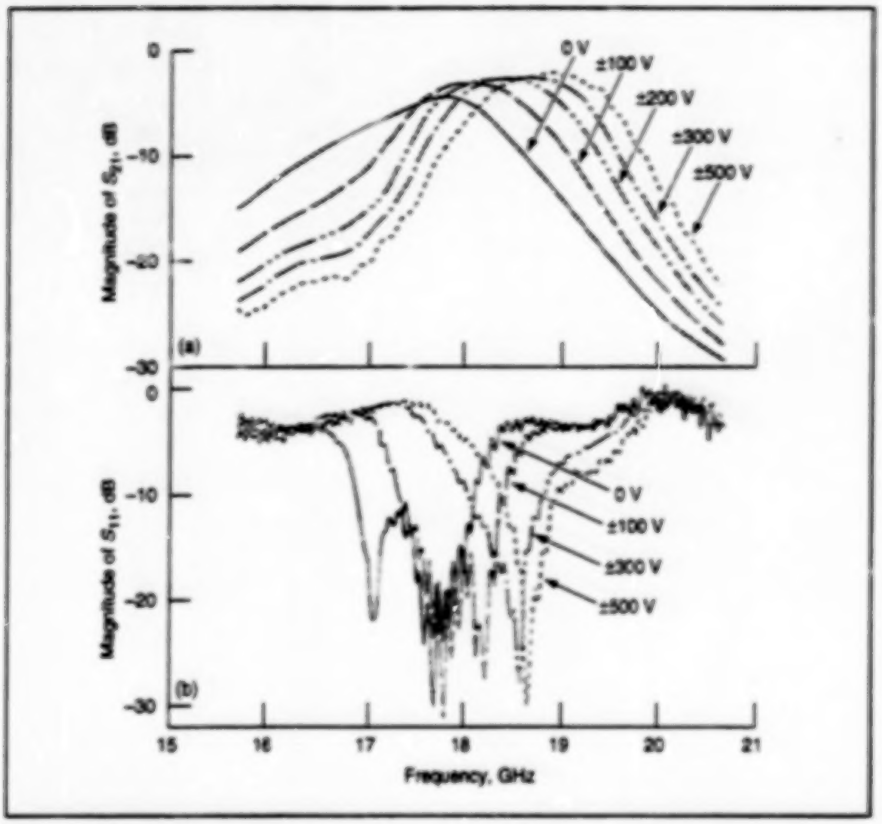

Figure 2. S_{11} and S_{12} of a Filter were measured at 77 K. These plots show the desired voltage dependence of the pass band, plus a desirable increase in S_{12} and a desirable decrease in S_{11} with bias voltage.

500 V, giving a tunability factor of 9 percent. The lowest measured pass-band insertion loss of this filter was 1.5 dB at 24 K. Another filter exhibited a tunability factor of 12 percent at a temperature of 30 K. In general, the return losses S_{11} and S_{22} of the filters were near or greater than 10 dB in the pass band. The resonance quality factor (Q) of the filters in the absence of loading was estimated to be ≈ 200. Efforts to optimize the HTS and ferroelectric films to obtain lower insertion losses and better tunability near 77 K and at lower bias voltages were underway at the time of reporting the information for this article.

This work was done by F. A. Miranda of **Glenn Research Center**, *F. Van Keuls of the National Research Council, and G. Subramanyam of the University of Northern Iowa. Further information is contained in a TSP [see page 1].*

Inquiries concerning rights for the commercial use of this invention should be addressed to NASA Glenn Research Center, Commercial Technology Office, Attn: Steve Fedor, Mail Stop 4–8, 21000 Brookpark Road, Cleveland, Ohio 44135. Refer to LEW-16751.

Current-Mode Dark-Level Subtraction in LWIR Imaging

This circuit offers high dynamic range and low noise.

NASA's Jet Propulsion Laboratory, Pasadena, California

A complementary metal oxide/semiconductor (CMOS) focal-plane readout circuit for an imaging array of long-wavelength infrared (LWIR) photodetectors effects in-pixel current-mode subtraction of the dark-level component of each photodetector output. The dark-level signal is subtracted before the signal reaches the integration node. Consequently, for each pixel in the array, the readout noise is minimized and the net gain and dynamic range are maximized.

This readout circuit was designed to overcome two major obstacles to the achievement of high performance in LWIR arrays used in imaging or spectroscopy under common operating conditions:

- Leakage in the photodetectors and/or high scene background gives rise to a large background signal, making it necessary for the focal-plane circuitry to handle of the order of several billion electron charges per pixel per readout cycle. Ordinarily, prohibitively large capacitors would be needed to handle such large amounts of charge, and the handling of large amounts of charge would introduce additional noise.
- Often, there is poor signal-to-background contrast in the sense that the signal of interest is of the order of only 10^{-4} or 10^{-3} times the background signal.

The present circuit operates in a readout cycle in which a blanking or calibration phase alternates with an imaging phase. During the blanking phase, a current-memory circuit memorizes the background current for use in predicting the background current for the subsequent imaging phase. During the imaging phase, the current-memory circuit acts as a high-impedance current source that generates the predicted background current, which is subtracted from the photodetector output current to obtain the signal current of interest. This signal current is coupled to external circuitry through low-noise circuitry, and an innovative biasing scheme improves low-noise performance.

A prototype of the circuit comprises a bilinear array of 2 × 132 multiplexers. Each unit cell (see figure) contains a LWIR photodetector [more specifically, a quantum-well infrared photodetector (QWIP)], a buffered-direct-injection (BDI) input circuit, a current-mode pedestal-subtracting circuit, and a voltage-mode double-sampled differential readout (DSDR) circuit. The BDI input circuit provides the stable bias needed for operation of the QWIP, plus a high input impedance that enables high quantum efficiency. The current-mode pedestal-subtracting circuit comprises a cascode current-memory circuit, and an isolation field-effect transistor (FET) denoted "M$_{read}$."

During the blanking phase, the current I_{det} flowing through the QWIP consist of the detector dark current (usually the dominant component, of the order of a few hundred nanoamperes) plus a smaller current due to scene and instrument background. I_{det} is the pedestal signal that one seeks to subtract. Ideally, once the current-memory circuit has memorized I_{det}, it should be able to generate $I_{mem} = I_{det}$.

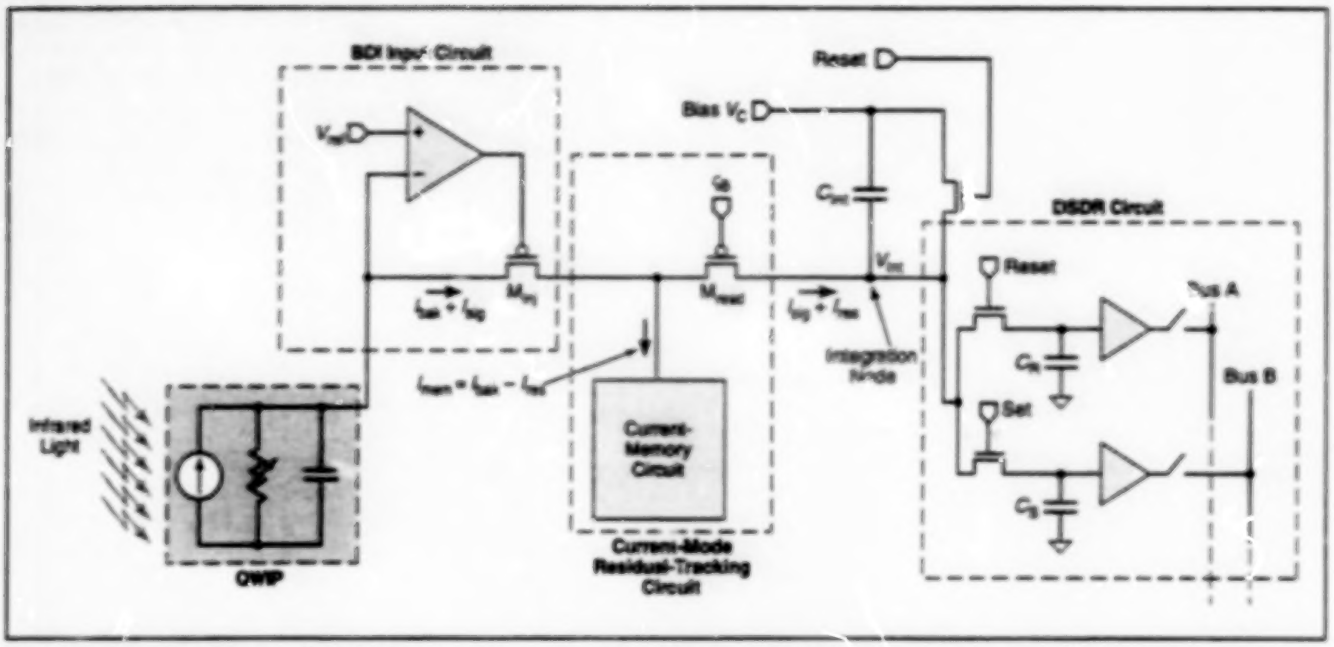

Each Unit Cell of the Readout Circuit effects in-pixel current-mode subtraction of the dark-level component of each photodetector output prior to integration.

However, because of imperfections in the circuit, I_{mem} and I_{bak} differ by a small amount: $I_{mem} = I_{bak} - I_{res}$, where I_{res} is denoted the error current. The pedestal signal due to I_{res} cannot be eliminated in the current-mode subtraction; therefore, it is estimated in the voltage mode by integrating the error current onto capacitor C_R in the DSDR circuit. This completes the memorization of the background signal.

During the imaging phase, the current through the QWIP rises above I_{bak} by an amount I_{sig}, which represents the infrared signal to be measured. Thus, the current sent to the integration node during the imaging phase equals $I_{sig}+I_{res}$. Once the imaging phase has been completed, the voltage V_{int} obtained by integrating $I_{sig}+I_{res}$ onto integration capacitor C_{int} is sampled on capacitor C_S in the DSDR circuit. As a result, the difference between the potentials on C_S and C_R is almost exactly proportional to I_{sig}, with background suppressed by factor of more than 10^4.

The gate of M_{read} is dc-biased with a voltage, such that during the blanking phase, the current-memory potential shuts M_{read} off, while during the imaging phase, the source of M_{read} charges up to a potential that enables the injection of current into the integration node. This biasing scheme makes it possible for the circuit to operate without need to apply a pulse signal ϕ_{read} to M_{read}. In so doing, the biasing scheme helps to keep noise low by preventing the injection of switching noise into a sensitive node.

The circuit provides for noise-limited measurement of signals 85 dB below the dark level. It is designed to operate with low power dissipation and high linearity, and is capable of handling pedestal currents up to 300 nA. Accurate subtraction of background charge makes possible a charge-handling capacity of $>5 \times 10^8$ electron charges per pixel.

This work was done by Bedabrata Pain, Guang Yang, Chao Sun, Timothy Shaw, and Chris Wrigley of Caltech for **NASA's Jet Propulsion Laboratory**. *Further information is contained in a TSP [see page 1].*
NPO-20486

Return-Link Processor PCI Card

Relative to prior return-link circuitry, this card is smaller, less power-hungry, higher performance, more versatile, and much cheaper.

Goddard Space Flight Center, Greenbelt, Maryland

The return-link processor card (RLP) performs all of the fundamental data-processing functions involved in the return of satellite telemetry, in real time at rates up to 400 Mb/s, using industry-standard interface circuitry and connectors with standard sizes and shapes. Previously, four cards, each containing a central processing unit (CPU), were needed to do what the RLP now does. CPU-based cards are complex, are expensive to build, operate, and maintain; are susceptible to malfunction; and require a great deal of power and cooling.

Functions of the RLP include frame synchronization, cyclic-redundancy-code and bit-transition-density decoding, detection and correction of errors by use of Reed-Solomon codes, processing according to the Consultative Committee for Space Data Systems (CCSDS) standard for Advanced Orbiting Systems (AOS) service, and CCSDS conventional processing of packets and frames of telemetric data. The RLP can also synchronize frames of data in a weather-satellite-data format and in other formats. Data received via the Internet and other low-rate sources accessible by a computer can be injected directly by the host computer in which the RLP is installed.

The RLP is a single industry-standard peripheral component interface (PCI) expansion card. In addition to the industry-standard PCI connector, it contains industry-standard subminiature B connectors for emitter-coupled-logic (ECL) input, an industry-standard DB-9 connector for RS-422 input, connectors for programming nonvolatile logic devices and a connector

for an optional sorting module (OSM — a mezzanine board on which additional buffering, processing, and output functions can be implemented.)

The RLP contains the following circuits:

- An ECL input interface circuit,
- An RS-422 input interface circuit,
- A special-purpose parallel integrated frame-synchronizing application-specific integrated circuit (ASIC),
- A special-purpose Reed-Solomon error-detecting-and-correcting ASIC,
- A custom ASIC for CCSDS AOS Service and conventional CCSDS processing of packets and frames,
- A PCI-bus-interface ASIC,
- A custom direct-memory-access interface reprogrammable, nonvolatile logic circuit,
- A custom reprogrammable nonvolatile logic circuit for monitoring and controlling the other circuits,
- A custom reprogrammable nonvolatile logic circuit that serves to collect status from the other circuits and supply it as a telemetry data stream, and
- Miscellaneous active and passive devices.

During typical operation, a standard serial data stream enters via either the ECL or the RS-422 input path, is processed in data-flow fashion through the ASICs, and is deposited in a number of first-in/first-out (FIFO) memory buffers onboard the RLP. Setup, control, retrieval of data, and monitoring are performed through an entirely memory-mapped PCI interface by software running on the host computer. The presence of data can be detected either by use of interrupts or by polling. Monitoring information is semiautomatically collected into easy-to-retrieve data blocks.

In comparison with the previous assembly of four cards, the RLP is smaller, less expensive, faster, and more energy-efficient. The CPU-less, memory-mapped mode of operation of the RLP is simpler and more robust than was the CPU-based operation of the previous assembly. The RLP is more flexible in that it can operate in any industry-standard PCI host computer and all logic is implemented in reprogrammable nonvolatile logic devices. The RLP is also both more flexible and expandable by virtue of the OSM interface connector.

This work was done by Kenneth B. Winiecki, Jason Dowling, Stephen T. Koubek, and Fred H. Peng of Lockheed Martin and Andrew F. Wolf of RMS for **Goddard Space Flight Center**. *Further information is contained in a TSP [see page 1].*

GSC-14032

Piezoelectric Igniter/Pressure-Sensor Devices

These devices would supplant conventional spark plugs in internal-combustion engines.

John H. Glenn Research Center, Cleveland, Ohio

Piezoelectric devices that would serve as spark plugs, power generators for spark plugs, and/or pressure sensors have been proposed for use in internal-combustion engines. Unlike conventional spark plugs, these devices would function without need for wire connections to external high-voltage sources. Also, unlike conventional spark plugs, these devices could function without need for external timing circuitry, and/or could function as parts of timing circuitry.

The most basic device of this type would be a self-timing, self-power-generating spark plug. The device would be mounted in a cylinder in an internal-combustion engine, in the manner of a conventional spark plug. The device would include a piezoelectric component with spark electrodes connected to its poles. The increase in pressure during the compression phase of the engine operating cycle would impose a strain on the piezoelectric component of the device and thereby give rise to a voltage between the electrodes. The voltage would increase with pressure until it was sufficient to cause a spark that would ignite the compressed fuel/air mixture in the cylinder. To increase the available voltage, the device could include a striker that would be driven by the increase in pressure to impinge on the piezoelectric component.

Immediately after ignition, the piezoelectric component would generate a voltage in response to the rapid increase in pressure associated with the combustion process. This voltage could be monitored to determine whether the engine is operating properly. The piezoelectrically generated voltage could also be monitored before as well as after sparking for more comprehensive monitoring of engine operation and, in particular, to detect such anomalies as pre-ignition, misfire, and knock.

The pressure-indicating piezovoltage could also be used, in conjunction with other indications of engine performance, to modify the spark timing. In a variation of the basic concept, the piezovoltage generated during the compression phase would initially be used to charge a capacitor; subsequently, under control by a timing circuit, the capacitor would be discharged through the spark electrodes. The spark timing could be in response to any combination of (1) the engine crank angle, (2) the pressure (as indicated by the piezovoltage), and (3) the rate of change of pressure.

This work was done by Jacob van Reenen Pretorius and Marthinus Cornelius van Schoor of Midé Technology Corp. for **Glenn Research Center**. *Further information is contained in a TSP [see page 1].*

Inquiries concerning rights for the commercial use of this invention should be addressed to NASA Glenn Research Center, Commercial Technology Office, Attn: Steve Fedor, Mail Stop 4–8, 21000 Brookpark Road, Cleveland, Ohio 44135. Refer to LEW-16780.

High-Power, Wideband Laser-Diode Transmitter Module

Diffraction-limited operation affords long range.

Goddard Space Flight Center, Greenbelt, Maryland

A prototype compact, rugged optomechanical module contains a high-power, wideband laser-diode transmitter. The laser diode is of a commercial single-quantum-well AlGaAs type. Each laser diode of this type is manufactured for a specific nominal wavelength in the range from 810 to 860 nm; the one in the prototype module lases at a nominal wavelength of 824 nm. The laser diode can be operated to emit continuous-wave power of 150 mW or with amplitude modulation at average and peak powers of 150 and 300 mW, respectively. The power consumption of the entire

module in dc operation is 400 mW. The laser diode is mounted on a copper plate, which conducts heat from the laser to a cold plate on which the module is mounted. The cold plate is maintained at a temperature of 15 °C.

A circuit board mounted on the copper plate next to the laser diode incorporates both dc and ac modulation electronics. Also included on the circuit board are a thermistor and a resistive heater for sensing and regulating the temperature of the laser diode. The modulation electronics include a reactive network matching circuit that enables the use of modulation frequencies up to a 3-dB-falloff frequency of 2.5 GHz. The laser diode, circuit board, and copper plate are all epoxied to a block of low-thermal-expansion glass, providing a stable platform from which to collimate and point the laser beam.

The laser diode emits a widely diverging, diffraction-limited, single-spatial-mode beam. A glass etalon in front of the laser provides wavelength-selective feedback and thus enables single-wavelength operation even in the presence of a large modulation signal. A molded glass aspherical lens with a focal length of 2 mm and an aperture diameter of f/1 roughly collimates the diverging laser beam to a divergence of about 0.5 by 1.5 milliradians. The roughly collimated laser beam also passes through a matched pair of lenses comprising a long-focal-length positive and a long-focal-length negative lens; the distance between these two lenses is adjusted to achieve fine adjustment of the collimation of the beam. The divergence achievable with fine adjustment of the collimation is low enough to make the laser beam useful at distances of the order of kilometers.

A pair of wedge prisms is used for fine adjustment of the pointing of the beam. A cubic beam splitter picks off a small fraction of the beam and directs it to another aspherical lens, which focuses this sample of the beam into a single-mode optical fiber for use in monitoring the modulation waveform or as a local-oscillator source for an optical receiver. To reduce the effects of optical feedback from the passive optical components into the laser, a quarter-wave plate is placed immediately after the first aspherical collimating lens and adjusted such that the polarization of any reflected light passing through is rotated to be orthogonal with the original polarization of the laser. Because the laser has almost no gain for this orthogonal polarization, the reflected light exerts no measurable effect on the laser.

This work was done by Donald M. Cornwell, Jr., and Pamela S. Millar of **Goddard Space Flight Center**, *Daniel X. Hoof of SSAI, and Anthony W. Yu of HSTX. Further information is contained in a TSP [see page 1].*
GSC-13824

Books and Reports

Studies of Interaction Impedance in a TWT Helix

Two reports present further developments in the subject of "Computation of Characteristics of a Helical TWT Slow-Wave Circuit" (LEW-16571), *NASA Tech Briefs*, Vol. 22, No. 4 (April 1998), page 54. The subject is computation, by use of the MAFIA (Solution of **MA**xwell's Equations by the **F**inite-**I**ntegration-**A**lgorithm) computer program, of the cold-test electromagnetic characteristics of the helix and surrounding structures in the slow-wave circuit of a traveling-wave tube (TWT). Special attention is given to the on-axis electron-beam/slow-wave interaction impedance, which cannot be measured directly. Heretofore, this impedance has been determined indirectly from cold-test measurement of the change in the resonance frequency resulting from the introduction of a dielectric rod on the axis. The equations used to obtain the interaction impedance from the measurement incorporate approximations (based on simplified geometry) that introduce errors. In the studies described in the two reports, it is shown that the interaction impedance can be determined accurately by modeling a TWT in its full three-dimensional complexity by use of MAFIA, and that doing so takes less time and costs less than does obtaining less-accurate information through a cold test.

This work was done by James A. Dayton, Jr., of **Glenn Research Center** *and Carol L. Kory of Analex Corp. To obtain copies of the reports, "Computational Investigation of Experimental Interaction Impedance Obtained by Perturbation for Helical Traveling-Wave Tube Structures," and "Accurate Cold-Test Model of Helical TWT Slow-Wave Circuits," see TSP's [page 1].*

Inquiries concerning rights for the commercial use of this invention should be addressed to NASA Glenn Research Center, Commercial Technology Office, Attn: Steve Fedor, Mail Stop 4–8, 21000 Brookpark Road, Cleveland, Ohio 44135. Refer to LEW-16881.

Hardware, Techniques, and Processes

Using Narrow-Band Data Links in Locating Lightning Strikes

Electric-field waveforms are preprocessed to extract selected characteristics.

John F. Kennedy Space Center, Florida

A method of preprocessing lightning-measurement waveforms has been devised to reduce the bandwidth needed to transmit data for computing the locations of lightning strikes. The method is used in a system in which electric fields and electric-field derivatives induced by lightning are measured at remote stations and the measurement data are transmitted to a central station. At the central station, the location of each lightning strike is computed from the known positions of the stations, the speed of light, and the differences among times of arrival of common waveform features at the remote stations. Prior to the development of the present method, in order to achieve a required spatial resolution of tens of meters, it was necessary to transmit full measurement data from each remote station to the central station in real time at a bandwidth of 10 MHz.

The preprocessing method exploits the following two concepts:

- A lightning strike typically comprises multiple strokes 20 to 50 ms apart, each stroke lasting of the order of 0.1 ms. Even during an intense thunderstorm, lightning strikes usually occur no more frequently than once every few seconds. Given this essential intermittency, the data-transmission bandwidth necessary to accommodate the time-averaged data rate is much less than the real-time, full-resolution bandwidth of 10 MHz. Thus, by abandoning real-time transmission, one can make possible a reduction in the data-transmission rate.
- If one extracts data on waveform characteristics that can be used to establish times of arrival, then the remaining waveform data can be discarded to effect a further reduction in bandwidth.

In this method, each remote station is equipped with a digitizer and an embedded controller. When a signal exceeds a predefined threshold, digital samples of the signal are taken at a rate of 20 megasamples per second for an observation interval of 100 μs. The record of samples is time-stamped with the starting time of the observation interval as determined by a differential Global Positioning System (GPS) receiver.

Still at each remote station, waveforms are characterized in terms of time elapsed between largest peaks (both positive and negative), rise times, durations at half maximum amplitudes, and other parameters. Each such characteristic is encoded in two bytes: one that identifies the characteristic and one that gives its value. The resulting code data and the time stamp are then transmitted to the central station for processing.

In the central station, the data from the remote stations are lined up in a search for matches among the characteristics. Differences among times of arrival are then determined on the basis of the best match.

The accuracy of the estimated differences among times of arrival increases with the number of characteristics. About 10 unique characteristics are enough to obtain good alignment. The bandwidth needed to transmit 10 coded characteristics and the accompanying timing data is 5 kHz — only 1/2,000th of the bandwidth needed for real-time transmission of full waveform data.

This work was done by Jose M. Perotti of **Kennedy Space Center** *and Pedro J. Medelius formerly of I-NET, Inc. Further information is contained in a TSP [see page 1].*

Inquiries concerning rights for the commercial use of this invention should be addressed to the Technology Programs and Commercialization Office, Kennedy Space Center, (407) 867-6373. Refer to KSC-11955.

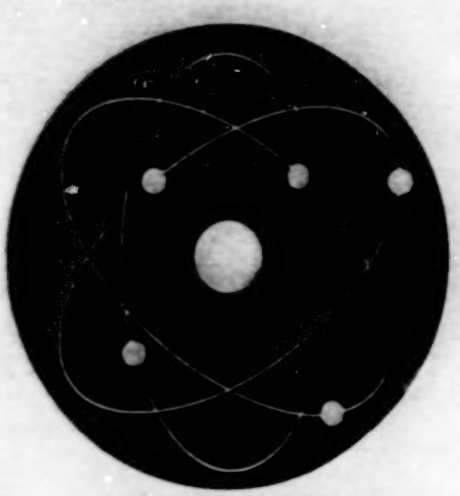

Physical Sciences

Hardware, Techniques, and Processes

Books and Reports

Temperature Correction for Pressure-Sensitive Paint

One can extract pressure data from partially-temperature-dependent luminescence data.

John H. Glenn Research Center, Cleveland, Ohio

A temperature correction has been developed to enable the extraction of pressure images and corresponding pressure data from images of photoluminescence of pressure-sensitive paints (PSPs). These paints are used on wind-tunnel models for mapping surface pressures associated with supersonic flow fields. PSP has been successfully used in wind-tunnel test ranging from 60 mi/h (97 km/h) to the supersonic range >3. The photoluminescence of an ideal PSP would depend on pressure only, but the photoluminescence of a real PSP depends on temperature also. In order to extract a pressure image, one must be able to invert the luminescence-image data on the basis, not only of the pressure dependence but also of the temperature dependence and of the distribution of temperature on the painted surface; in other words, one needs to incorporate a temperature correction into the pressure calibration of the luminescence of the paint.

A PSP contains luminophores (basically, dye molecules), that luminesce in a suitable wavelength range in response to photoexcitation in a shorter wavelength range. The photoluminescence is quenched by oxygen at a rate proportional to the partial pressure of oxygen and thus proportional to the pressure of air. As a result, the intensity of photoluminescence varies inversely with the pressure of air, and the basic equation for calibrating a photoluminescence image is the following:

$$P/P_{REF} = A + BI_{REF}/I,$$

where P is the unknown pressure that one seeks to determine under the test condition (e.g., in the presence of wind), P_{REF} is the pressure under a reference condition (e.g., in the absence of wind), I_{REF} is the intensity of luminescence under the reference condition, and I is the intensity of luminescence under the test condition. The need for temperature correction arises because A and B depend on temperature.

The temperature correction is based on the experimental observation that in the above equation for P/P_{REF}, the combined effects of pressure and temperature can be expressed by use of a corrected intensity ratio; that is,

$$P/P_{REF} = A + B(I_{REF}/I_{CORR}.$$

The corrected intensity ratio is given by

$$I_{REF}/I_{CORR} = I_{REF}/I)(CT^2+DT+E),$$

where T is the absolute temperature and C, D, and E are constants obtained via a least-squares best fit to calibration data acquired by use of a PSP test rig. Alternatively, calibrations usually use a combination of PSP calibration cell data and conventional pressure taps. The taps are used as truth points to help set an absolute level since this is a delta (change) pressure measurement and the largest error is typically the absolute pressure level. The figure presents calibration plots for a PSP, as they appear before and after the application of the temperature correction.

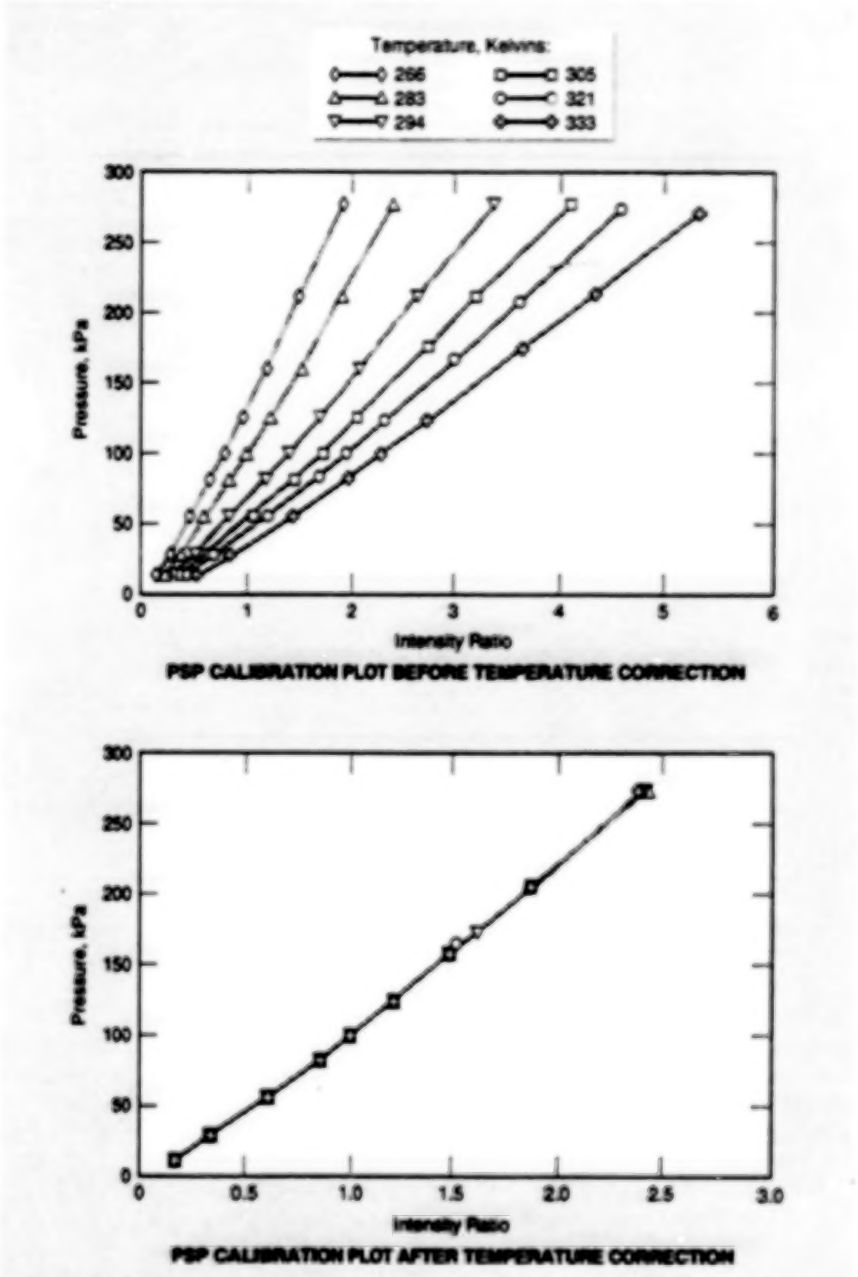

A Family of Calibration Curves clearly depicts the effect of temperature. The temperature correction collapses the family of curves to a single curve, so that it suffices to perform the pressure calibration at one temperature only.

Of course, in order to be able to apply the temperature correction to PSP images of a model in a wind-tunnel test, one must know the temperature distribution on the model during the test. A temperature image can be acquired by coating the model with a temperature-sensitive paint (TSP) and testing it under the same conditions as those used when it is coated with

PSP. Alternatively, this can help for a uniform temperature change but does not help for correcting for temperature gradients on the test article. Large temperature gradients exist on thermally conductive models that need full field temperature measurements to fully compensate for the temperature sensitivity of PSP.

This work was done by Timothy J. Bencic of **Glenn Research Center**. *Further information is contained in a TSP [see page 1].*

Inquiries concerning rights for the commercial use of this invention should be addressed to NASA Glenn Research Center, Commercial Technology Office, Attn: Steve Fedor, Mail Stop 4-8, 21000 Brookpark Road, Cleveland, Ohio 44135. Refer to LEW-16915.

Lightweight, Low-Power, Inexpensive Ozone Dosimeters

Ozonolysis of organic dyes would cause color changes, which would be measured.

NASA's Jet Propulsion Laboratory, Pasadena, California

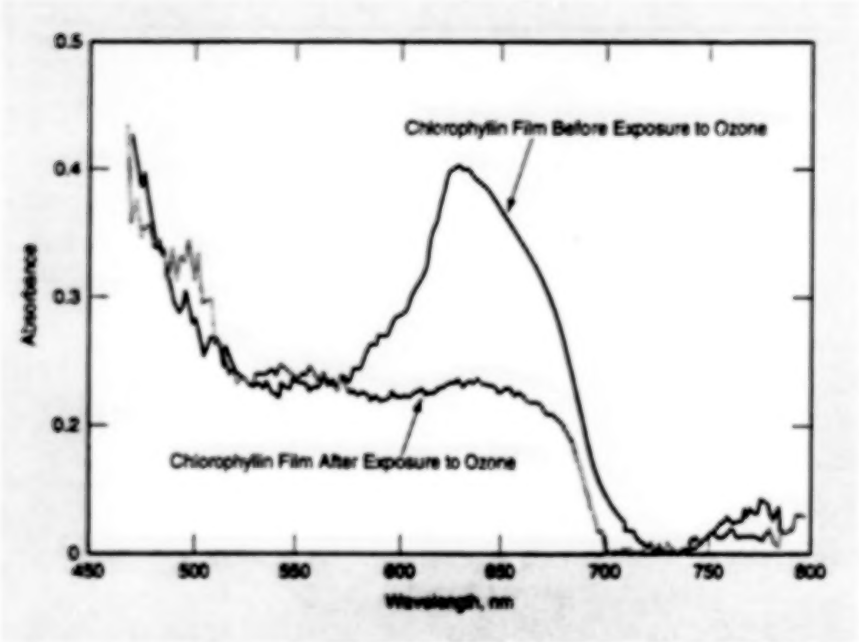

The Absorbance of a Chlorophyllin Film on a glass slide was measured before and after exposure to ozone. The fall of the 630-nm peak and the rise of the 500-nm peak can be interpreted in terms of ozone dosage.

Lightweight, low-power-consumption, inexpensive ozone sensors based on colorimetric chemical sensing would be developed, according to a proposal. Colorimetric chemical sensing is an established technique, but it has not been applied previously to sensing of ozone. The proposed ozone sensors could be incorporated into radiosondes for measuring tropospheric and stratospheric ozone concentrations; they could also be used to monitor ozone in a variety of indoor and outdoor environments near such ozone sources as electric-arc welding equipment, high-voltage laboratory instruments, photocopiers, laser printers, and electrostatic air cleaners.

An ozone sensor as proposed would include a transparent substrate (e.g., a glass or plastic slide) coated with an organic dye that changes color when it reacts chemically with ozone. The coated substrate would be illuminated by one or more light-emitting diode(s) or diode laser(s) of the appropriate wavelength(s), and the portion of incident light transmitted through the coated substrate at each wavelength of interest would be measured by a photodiode. The color change would manifest itself as a change in absorbance, and thus a change in the amount of transmitted light at each wavelength of interest. A change in absorbance at each wavelength of interest would be related to the degree of reaction and thus to the ozone dosage via the Beer-Lambert law:

$$A = \alpha l c = \ln(I/I_0),$$

where A is the change in absorbance, α is the dosage-dependent change in the absorption coefficient of the dye, l is the thickness of the layer that contains the dye, c is the concentration of the dye in the layer, I_0 is the intensity of transmitted light before exposure to ozone, and I is the intensity of transmitted light after exposure to ozone.

An ozone sensor should operate without interference by oxidizing substances other than ozone (e.g., halogens, SO_2, and NO_2). Therefore, the dye should be either one that does not exhibit color changes in the presence of the other substances, or else one for which the color change induced by ozone differs measurably from the color change(s) induced by the other substances. A promising dye of the latter type is chlorophyllin — a copper-containing, water-soluble derivative of chlorophyll.

Chlorophyllin exhibits an absorption peak at a wavelength of 630 nm. This peak diminishes in proportion to the degree of reaction (see figure), making it possible to quantify the ozone dosage via the Beer-Lambert law. In addition, the product of ozonolysis of an ethylene group on the chlorophyllin molecule gives rise to a smaller absorption peak at 500 nm; the corresponding absorption peaks induced by other oxidizing species occur at different wavelengths. Thus, one could use the 500-nm peak to verify that the observed color change was caused by ozone or, alternatively, one could identify the oxidizing species by measuring the different wavelength of this peak.

Because the color change would be irreversible and proportional to the cumulative exposure to ozone, a sensor of this type would be a dosimeter (as distinguished from a concentration meter). However, it may be possible to determine the instantaneous concentration of ozone from the rate of change of the absorbance.

This work was done by Margie Homer, Margaret A. Ryan, and Roger Williams of Caltech for **NASA's Jet Propulsion Laboratory**. *Further information is contained in a TSP [see page 1].*

NPO-20469

Telescope for Imaging and Laser Communication

Light is transmitted and received through the same objective lens.

NASA's Jet Propulsion Laboratory, Pasadena, California

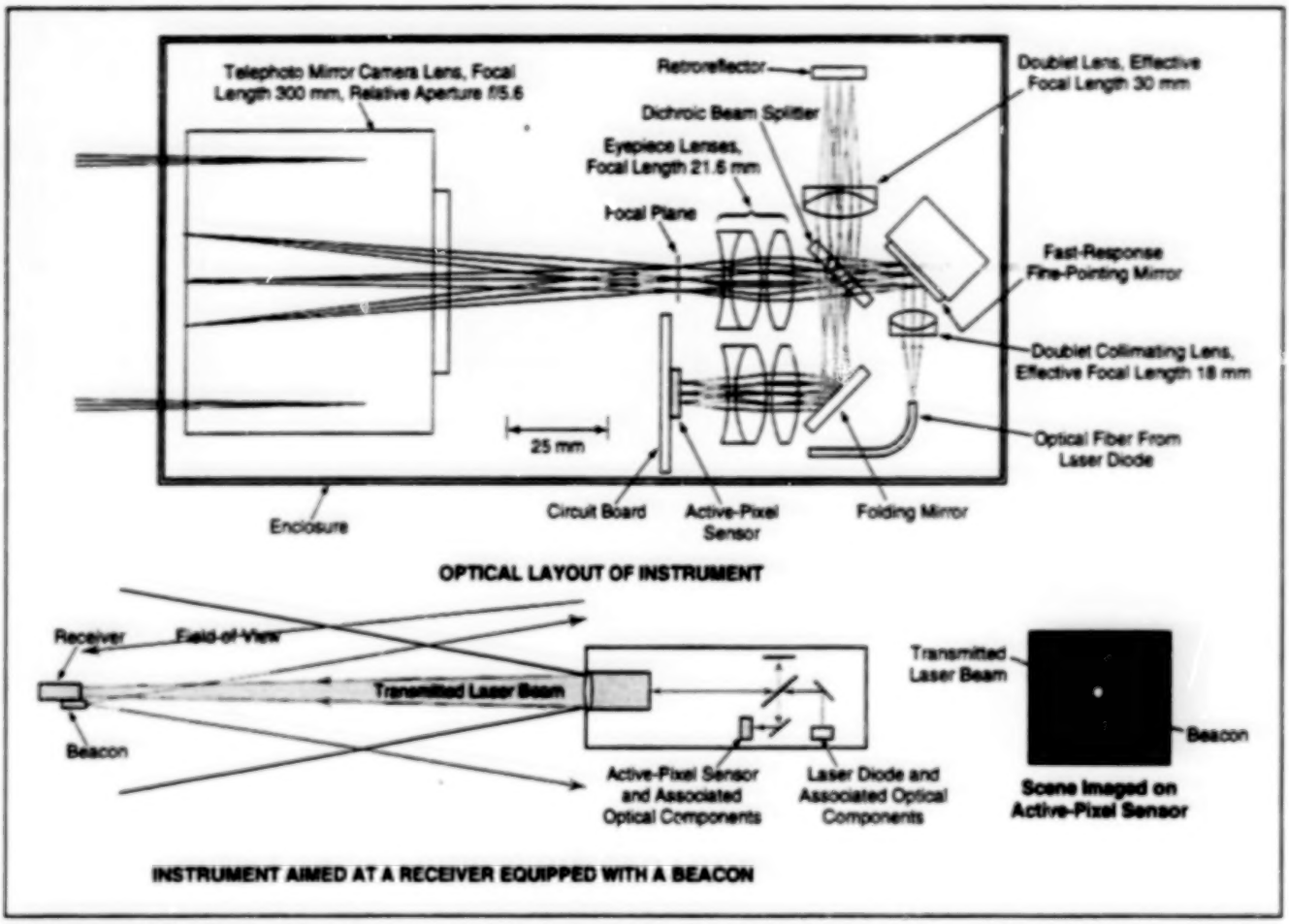

This **Instrument Can Be Used** for both imaging and laser communication. The imaging function is also used to aim the instrument for laser communication.

Miniature, single-aperture optoelectronic instruments called "multi-function telescopes" are being developed for use in both scientific observations and laser communications aboard microspacecraft that are expected to be launched in the next few years. These instruments could also be adapted to imaging and communication applications on Earth.

As now envisioned, a multi-function telescope would serve as (1) a conventional telescope for scientific imaging, (2) a telescope for celestial navigation, (3) an infrared spectrometer, and (4) a laser communication system. A prototype multi-function telescope called "a combined laser-communication and imager for microspacecraft" (ACLAIM) has been built and tested to demonstrate two of these functions: laser communication and scientific imaging. The prototype instrument was assembled from mostly commercially available parts.

The figure schematically depicts the prototype instrument. All incoming and outgoing light passes through telephoto mirror camera lens. Within the instrument, there are three partly overlapping optical channels: a receiving channel, a transmitting channel, and a boresight channel. The three channels intersect at a dichroic beam splitter, which makes it possible to use the same path through the telephoto lens for both receiving and transmitting.

The receiving channel extends from the telephoto lens to the beam splitter to an Active-Pixel Sensor (APS). Light to be transmitted is generated by modulating the power supplied to a laser diode equipped with a pigtail optical fiber, and the transmitting channel is considered to extend from the output end of the optical fiber to the beam splitter, then from the beam splitter out through the telephoto lens. The beam splitter exhibits high reflectance at wavelengths from 500 to 900 nm, except in a 40-nm-wide band at the laser wavelength of 670 nm, where it exhibits 70-percent transmittance.

The boresight channel includes a retroreflector, which sends a small portion of the laser beam to the APS. A laser beacon at a distant receiver is also imaged onto the APS. The positions of the spots of light from the beacon and the laser beam are measured and used to compute the angle between the transmitted beam and the line of sight to the beacon.

In the original intended use aboard a spacecraft, the spacecraft would be turned to aim the telescope at an astronomical target of scientific interest and image data would be acquired by use of the APS. The image data would be stored in memory for subsequent transmission to the distant receiver via modulation on the outgoing laser beam.

In preparation for transmitting the image data, the spacecraft and telescope would

be turned to bring the beacon at the receiver within the field of view of the telescope. Then a control system would adjust the orientation of the spacecraft and of a fast-response fine-pointing mirror in the instrument, in response to the angle measured as described in the preceding paragraph. The techniques for measuring the angle and aiming the telescope were described in more detail in three previous articles in *NASA Tech Briefs*: "Beam-Steering Subsystem for Laser Communication" (NPO-19069), Vol. 19, No. 6 (June 1995), page 32; "Digital Controller for Laser-Beam-Steering Subsystem" (NPO-19193), Vol. 19, No. 11 (November 1995), page 93; "More About Beam-Steering Subsystem for Laser Communication" (NPO-19381), Vol. 19, No. 11 (November 1995), page 93; and "Image Processing in Laser-Beam-Steering Subsystem" (NPO-19396), Vol. 20, No. 5 (May 1996), page 24.

This work was done by Hamid Hemmati and James Lesh of Caltech for **NASA's Jet Propulsion Laboratory**. *Further information is contained in a TSP [see page 1].*

In accordance with Public Law 96-517, the contractor has elected to retain title to this invention. Inquiries concerning rights for its commercial use should be addressed to

Technology Reporting Office
JPL
Mail Stop 122-116
4800 Oak Grove Drive
Pasadena, CA 91109
(818) 354-2240

Refer to NPO-20388, volume and number of this NASA Tech Briefs *issue, and the page number.*

Method of Measuring Encircled Energy for Imaging Optics

Micromachined apertures are precisely, concentrically interchanged in focal planes.

Goddard Space Flight Center, Greenbelt, Maryland

The radial distribution of energy within an image, called encircled energy, is a classical measure of the quality of the optical system producing that image. An improved method for measuring encircled or enclosed energy for imaging optical systems makes use of precisely micromachined apertures which are positioned with great accuracy at the center of an image.

The technique is an improved solution to the problem of measuring radiant fluxes passing through a sequence of round or square holes of progressively increasing size, all centered on the same point of interest in a focal plane of the optical system. The sequence of measurements determines the radial distribution of irradiance about the point of interest. This distribution is useful for specifying and characterizing the performance of the optical system; in particular, if the point of interest is the nominal center of the image of a bright point object, then the desired distribution is related in a known way to the point-spread function of the system.

The concept of using progressively wider apertures of identical shape to measure the radial distribution of irradiance is so straightforward as to seem almost trivial; however, in practice, it has historically proven difficult to implement this concept with the precision needed to characterize the performances of advanced vacuum-ultraviolet and x-ray imaging instruments. The difficulty lies in being able to interchange each aperture exactly concentrically and in focus, especially with a collection of discrete apertures. Alternative methods which involve knife-edge or slit scanning are always indirect approaches to measuring encircled energy and produce somewhat ambiguous results.

The new method affords all of the necessary precision. An opaque mask containing a linear array of identically-shaped but differently-sized apertures has been fabricated by chemical micromachining in a thin, flat silicon substrate. Also fabricated during the micromachining process are a set of binary-coded fiducial marks — one mark for each aperture, located at a known distance well to the side of the aperture. The precision of dimensions and locations of apertures and fiducial marks are of the order of 0.1 to 0.2 μm — commensurate with the state of the art of microlithography. Aperture sizes progress slowly from 1 μm all the way up to 2 mm in both circular and square aperture shapes.

The aperture mask is mounted in front of a photodetector on a translation stage with three mutually orthogonal axes with 0.1-μm position resolution — one for motion perpendicular to the focal plane (focus) and two for motion within the focal plane.

The linear array of apertures is carefully mounted so as to be parallel to the direction of travel of one of the latter motions. The exact position of the selected aperture of interest in the focal plane is sensed by using an optoelectronic apparatus to measure the position of the associated fiducial mark. A lens focuses a magnified image of the backlit fiducial mark onto a small, charge-coupled-device (CCD) image detector. The CCD output is digitized and processed to decode the binary pattern (and thereby the selected aperture) and to determine the position of the aperture to within about 0.01 μm.

In preparation for the measurement process, a photodetector wider than the focal spot of interest is positioned just behind the focal plane to intercept the focused light. The largest aperture in the aperture mask is centered approximately on the image, then moved from side to side along both image-plane axes while observing the photodetector output to find the points, corresponding to passage of the aperture edge, beyond which the light is totally blocked. The center of the image is tentatively deemed to lie halfway between the extinction points on the two axes. To locate the center of the image with progressively increasing precision, this procedure is repeated with the next smaller aperture, and so forth down to the smallest aperture. Then a final precise centering operation is performed by searching for the maximum photodetector output or other suitable indication while using the smallest aperture.

Once the center has been located, the encircled-energy measurement begins with the recording of the photodetector response with the smallest aperture in place. Then the responses are recorded with successively wider apertures, using the translation stage and fiducial marks to ensure the concentricity of each successively selected aperture. The photodetector responses thus recorded constitute the desired raw encircled-energy data.

This work was done by Douglas B. Leviton and Sridhar M. Manthripragada of **Goddard Space Flight Center**. *Further information is contained in a TSP [see page 1].*

GSC-13872

Liquid-Feed Methanol/Hydrogen Peroxide Fuel Cell

The difficulties and hazards of gaseous feeds are eliminated.

NASA's Jet Propulsion Laboratory, Pasadena, California

The figure schematically illustrates a fuel cell that consumes methanol and oxygen from hydrogen peroxide, with both fuel and oxidant supplied in aqueous solutions. Unlike fuel cells that consume either pure hydrogen and oxygen gases or else pure hydrogen plus oxygen from air, fuel cells like this one can be operated without the difficulties of storing and handling compressed gases. In comparison with pure hydrogen and oxygen gases, the aqueous fuel and oxidant solutions used in these liquid-feed fuel cells pose less of an explosion hazard, making these fuel cells more suitable for use in confined spaces. Yet another advantage for operation in confined spaces is that unlike some other fuel cells, these fuel cells can be operated without depending on possibly limited volumes of ambient air for oxygen supplies.

The heart of this and other similar fuel cells is a membrane/electrode assembly that includes a proton-conducting polymer-electrolyte membrane sandwiched between two catalytic electrodes. Each electrode comprises a outer porous, electrically conductive layer and a catalytic layer. The aqueous solution containing methanol is circulated past the electrode on one side of the membrane; the aqueous solution containing hydrogen peroxide is circulated past the electrode on the other side of the membrane. The catalyst for the electro-oxidation of methanol is a Pt/Ru alloy; the catalyst for the electro-reduction of hydrogen peroxide is Pt.

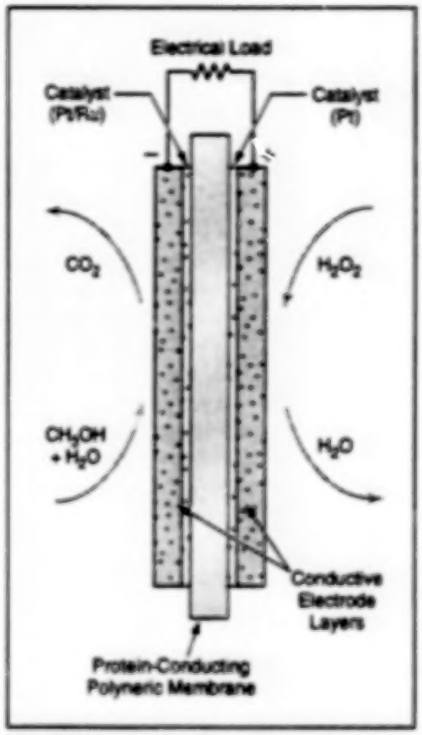

The **Reactants Are Supplied in Aqueous Solution** entirely, making it unnecessary to store or handle compressed gas.

The electrode that sustains the electro-oxidation of methanol becomes the negative electrode, while the electrode that sustains the electro-reduction of hydrogen peroxide becomes the positive electrode. The chemical reactions are the following:

$$CH_3OH + H_2O \rightarrow CO_2 + 6H^+ + 6e^-$$

at the negative electrode and

$$H_2O_2 + 2H^+ + 2e^- \rightarrow 2H_2O$$

at the positive electrode. Thus, the only net products of the chemical reactions are CO_2 and H_2O.

A prototype of this liquid-feed fuel cell was tested, using an aqueous methanol solution with a concentration between 0.5 and 1 molar and an aqueous hydrogen peroxide solution with a concentration of 5 volume percent. In the tests at temperatures from 22 to 42 °C, the cell was found to sustain an areal power density of several tens of milliwatts per square centimeter; this is about one-third the areal power density of a typical methanol fuel cell that consumes pure oxygen gas, but it should be possible to increase the power density by increasing the concentrations of methanol and hydrogen peroxide and operating at higher temperature.

This work was done by Sekharipuram Narayanan, Thomas I. Valdez, and William Chun of Caltech for **NASA's Jet Propulsion Laboratory**. *Further information is contained in a TSP [see page 1].*

NPO-20249

High-Temperature Pressure Sensors Made From Silicon Carbide

Working temperatures range up to 500 °C.

John H. Glenn Research Center, Cleveland, Ohio

Pressure sensors that contain thin diaphragms made from the 6H polytype of silicon carbide (6H-SiC) have been developed. These are prototypes of pressure sensors for use at high temperatures in engines, power plants, material-processing systems, and numerous other applications.

The wide band gap (3.0 V), high breakdown electric field (2.5 MV/cm), and high electron saturation speed (2×10^7 cm/s) of 6H-SiC make it a superior candidate material for high-temperature electronic devices. In addition, SiC exhibits excellent thermal and mechanical properties at high temperatures and large coefficients of piezoresistance — a combination of properties that makes this material suitable for high-temperature electromechanical sensors.

The prototype SiC pressure sensors were batch-fabricated by micromachining and demonstrated to work at temperatures from room temperature up to 500 °C. The 6H-SiC starting material (i.e., wafers) have micropipes in them. The processing conditions applied in this work plugged the micropipes, thereby making the 6H-SiC material useable.

The SiC pressure sensors offer the following five major advantages in addition to those mentioned above:

1. Junction leakage, which renders silicon semiconductor devices inoperative at high temperatures, is insignificant because of the wide band gap of 6H-SiC.
2. The low hole mobility [50 cm2/(V-s)] of a lightly-p-doped diaphragm makes the diaphragm highly resistive to planar electric current.
3. Because the results of bulk micromachining are reproducible, batch production offers advantages of low cost, short processing time, and high yield.
4. Because of the homogeneity of bulk micromachined 6H-SiC, these pressure sensors are not subject to the adverse effects of thermal-expansion mismatches, which can be problematic in devices made from heterogeneous materials.
5. Plastic deformation of SiC is not known to occur at the upper end of the temperature range of interest. Consequently, the diaphragms in these sensors remain effective force collectors, even at this high temperature.

This work was done by Anthony A. Ned, Anthony D. Kurtz, and Robert S. Okojie of Kulite Semiconductor Products, Inc., for **Glenn Research Center**. *Further information is contained in a TSP [see page 1].*

Inquiries concerning rights for the commercial use of this invention should be addressed to NASA Glenn Research Center, Commercial Technology Office, Attn: Steve Fedor, Mail Stop 4–8, 21000 Brookpark Road, Cleveland, Ohio 44135. Refer to LEW-16772.

Books and Reports

Techniques for Controlling Buoyancy of Balloons on Titan

A report discusses alternative techniques for controlling the buoyancy, and thus the attitude and landings, of a balloon-borne instrumentation system that would be launched to explore the moon Titan of the planet Saturn. Some of the techniques are based on established concepts of heating or cooling gases in balloons. One technique involves the acquisition or release of gaseous ballast by compressing and liquefying atmospheric gas into a pressure vessel (or allowing the liquefied gas to vent back to the atmosphere); a similar technique involves compressing atmospheric gas into (or releasing it from) a bladder. Another technique involves filling a balloon with a fluid that undergoes altitude-dependent phase changes. Another technique is one for acquiring ballast by use of a material that, at ambient temperature, would adsorb a mass of atmospheric gas somewhat greater than the mass of the sorbent, thereby decreasing buoyancy and causing descent. Heating the sorbent would release the gas, thereby decreasing the mass of the balloon system and increasing buoyancy to cause ascent. The simplest and preferred buoyancy technique is to use controlled heating of the helium balloon by means of diverting waste heat from a radioisotope thermoelectric power source.

This work was done by Jack Jones and Jay Wu of Caltech for **NASA's Jet Propulsion Laboratory**. *To obtain a copy of the report, "Preliminary Study of Titan Balloon Buoyancy Techniques," see TSP's [page 1].*

NPO-20656

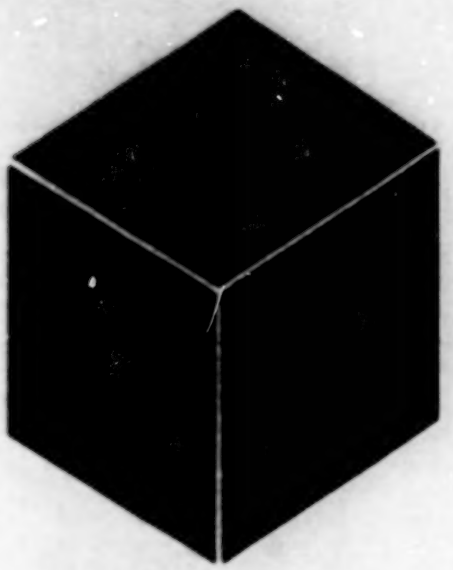

Materials

Hardware, Techniques, and Processes

Books and Reports

Reducing Methanol Crossover in CH_3OH-Fuel-Cell Membranes

Perfluorosulfonic acid-based membranes are impregnated with poly(styrene/divinylbenzene).

John H. Glenn Research Center, Cleveland, Ohio

Improved polymer electrolyte membranes for direct methanol fuel cells can be made by impregnating the baseline membrane material with cross-linked polystyrene (a copolymer of styrene and divinylbenzene). The baseline membrane material is a perfluorosulfonic acid-based hydrophilic, proton-conducting ion-exchange polymer sold under the trade name "Nafion". The principal benefit afforded by the impregnation is a reduction in permeability by methanol; this translates to less crossover of methanol in molecular form (denoted "methanol crossover" for short). Methanol crossover is undesired because it wastes fuel and thereby degrades fuel-cell performance.

To demonstrate this concept, membranes were prepared as follows:

1. Baseline membranes were cut slightly larger than the final size needed for fuel-cell membrane/electrode assemblies (MEAs). The membranes were dried, weighed, and marked for identification.
2. Solutions of 1, 3, 5, and 8 weight percent styrene/divinylbenzene in methyl chloride with 1 weight percent benzoyl peroxide as an activator were prepared for use in impregnation and polymerization.
3. The membranes were placed in the solutions in test tubes, which were then capped to prevent exposure to air.
4. Each capped test tube was heated to a temperature between 60 and 65 °C for 16 or more hours, until polymerization was complete.
5. After cooling to room temperature, the test tubes were cracked to remove the styrenated membranes.
6. Excess polystyrene (the portion not cross-linked with the baseline membranes) was removed by immersing the samples in methyl chloride at room temperature for various times ranging from 1 to 24 hours.
7. The styrenated membranes were sulfonated by immersing them in a solution of $ClSO_3H/CH_3Cl$ for 16 hours.
8. The sulfonated membranes were placed in distilled water at room temperature, the beaker was covered, and the water was brought to a rapid boil. Samples of the water were cooled to room temperature and tested for Cl^- ions by use of one or two drops of $AgNO_3$ solution. In each case, if a positive result was found, the membranes were removed and placed into another, previously heated beaker of distilled water. This was repeated until the test for Cl^- ions yielded a negative result.

Membrane Material	Cell Potential (mV) at Current Density of:		Crossover, Percent	Electrical Resistance (mΩ) at a Temperature of 60 °C
	100 mA/cm²	200 mA/cm²		
Baseline	530	450	19.5	7.2
Baseline Containing 8 Weight Percent Cross-Linked Polystyrene	450	290	15.6	10.5

These Fuel-Cell Performance Figures were obtained using MEAs containing two different membranes.

Both baseline membranes and membranes prepared as described above were tested to characterize them with respect to ion-exchange capacity, water content, cell resistance, permeability by methanol, and proton conductivity. The best one of the prepared membranes was fabricated into a complete MEA, using Pt/Ru anode and Pt black cathode catalysts. An MEA was also made from a baseline membrane. Both MEAs were then tested in a fuel cell. The results of the test (see table) show decreased methanol crossover in the case of the styrenated membrane. The results also show decreased fuel-cell performance in this case. The decrease in performance has been tentatively attributed to incompatibility of the styrenated membranes with the electrode structures and bonding conditions, which were optimized for the unstyrenated membranes. The implication is that it should be possible to recover lost fuel-cell performance by optimizing the electrode structures and bonding conditions for styrenated membranes.

This work was done by J. Kosek, M. Hamdan, and A. B. LaConti of Giner, Inc., for **Glenn Research Center**. *Further information is contained in a TSP [see page 1].*

Inquiries concerning rights for the commercial use of this invention should be addressed to NASA Glenn Research Center, Commercial Technology Office, Attn: Steve Fedor, Mail Stop 4–8, 21000 Brookpark Road, Cleveland, Ohio 44135. Refer to LEW-16669.

Composite-Material Heat Sink for Printed-Circuit Boards

This is a lightweight alternative to an aluminum heat sink.

Goddard Space Flight Center, Greenbelt, Maryland

A laminated composite-material plate has been developed for use as a lightweight heat sink and mechanical support for rigid printed-circuit boards (PCBs) that hold surface-mounted electronic components. This composite-material plate is intended to replace a conventional aluminum heat-sink plate. The aluminum plate weighs 0.63 lb (0.29 kg), whereas the composite-material plate weighs only 0.36 lb (0.16 kg).

An advanced laminated composite is attractive as an alternative to aluminum in several respects:

- The orientations of fibers in the laminae can be selected to tailor the properties of the laminate.
- The bending stiffness of a typical advanced laminated composite material is eight times as great as that of aluminum; this is an important advantage because PCBs that hold surface-mounted components are relatively intolerant to flexing. (The intolerance to flexing arises because flexing can break the beads of solder used for attachment in surface mounting.)
- The density of a typical advanced composite material is two-thirds that of aluminum.
- The coefficient of thermal expansion (CTE) of a quasi-isotropic composite laminate is typically less than one-eighth

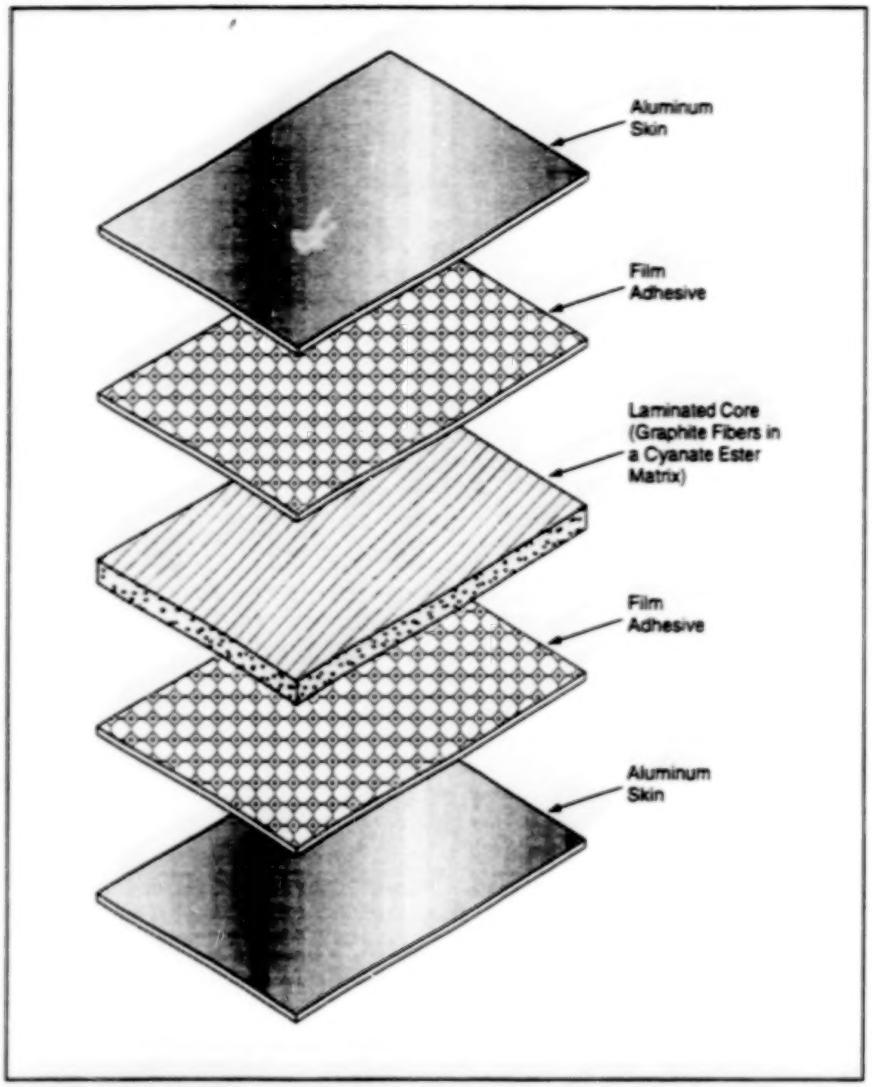

The **Composite Heat Sink** was designed to satisfy strength, stiffness, and heat-transfer requirements at least as stringent as those imposed on the design of an aluminum heat sink, but to weigh 43 percent less than the aluminum heat sink does.

that of aluminum. The lower CTE of the composite material, in concert with the CTE of the PCB material, promises an increase in fatigue lives of solder joints, and thus increased reliability.

- The effective thermal conductivity of an advanced composite material can be made to exceed that of aluminum; as a result, better heat-sink performance is attainable. As a consequence of better heat-sink performance, heat-generating components can be packed more densely; thus, a greater degree of miniaturization is possible.

The composite-material heat-sink plate (see figure) comprises (1) a quasi-isotropic laminated core of graphite fibers in a cyanate ester matrix and (2) a 0.002-in. (0.05-mm)-thick aluminum skin backed with a film adhesive. The laminated core consists of six laminae; the quasi-isotropy is achieved by stacking each lamina with its fibers at an angle of 60° with respect to those of the adjacent lamina. This fiber orientation was chosen because it optimizes the strength and stiffness characteristics of the laminate. Because the thermal conductivity is greatest along the fibers and it is desired to maximize widthwise thermal conduction in the heat sink, the fibers in the 0° plies are oriented along the width of the heat sink. The aluminum skin is wrapped around the laminated core to provide a continuous ground plane for the PCBs.

This work was done by Jill M. Holz, Lee Niemeyer, and David Puckett of **Goddard Space Flight Center**. *Further information is contained in a TSP [see page 1].*
GSC-14142

Books and Reports

Update on Electrolytes for Low-Temperature Lithium Cells

A report presents results of research on carbonate-based electrolytes to improve the low-temperature-performances of lithium-ion rechargeable electrochemical cells. From earlier research, it was determined that the loss of performance with decreasing temperature is attributable largely to a decrease of ionic conductivity and the increase in viscosity of the electrolyte. What is needed to extend the minimum operating temperature from 20 °C down to –40 °C is a stable electrolyte solution with relatively large low-temperature conductivity, relatively small low-temperature viscosity, a large electric permittivity, adequate coordination behavior, and appropriate ranges of solubilities of liquid and salt constituents. One electrolyte found to yield excellent room- and low-temperature performance is a 1.0 M solution of $LiPF_6$ in a solvent that consists of equal volume parts of ethylene carbonate, dimethyl carbonate, and diethyl carbonate. Prototype cells that contained this electrolyte exhibited high charge and discharge capacities at temperatures from –20 to –40 °C, capability for discharge at high rates, and high cycle lives at both low and room temperatures.

This work was done by Marshall Smart, Ratnakumar Bugga, Chen-Kuo Huang, and Subbarao Surampudi of Caltech for **NASA's Jet Propulsion Laboratory**. *To obtain a copy of the report, "Rechargeable Lithium-Ion Cells with Improved Low-Temperature Performance with Novel Carbonate-Based Electrolyte," see TSP's [page 1].*
NPO-20407

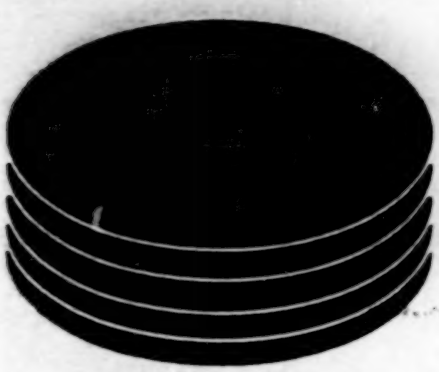

Computer Programs

Materials

Materials

The Automated Fatigue Calculation Program (FATPLUS)

This is a menu-driven, interactive program that performs multiple functions.

Since it was developed in the late 1980s, the Automated Fatigue Calculation Program (FATPLUS) has consistently demonstrated its ability to predict fatigue life, independently validate proprietary fatigue methodologies, identify fatigue-sensitive parts, and train engineers in predicting fatigue lives. FATPLUS enables its users to create, save, and modify specific stress spectra and properties of materials.

A conservative methodology yields valid estimates of fatigue lives as long as reasonable engineering practices are maintained. However, FATPLUS can do more than this. The program is also a powerful, menu-driven, interactive design software tool for studying and analyzing effects of a spectrum of stresses, effects of changes in design, effects of changes in materials, and changes in concentrations of stresses.

To make FATPLUS into a program that predicts fatigue lives and a very powerful tool for analyzing systems, the developers of FATPLUS accounted for (1) the spectrum of stresses, (2) the number of loadings per stress event, (3) fatigue properties of materials, and (4) safety factors. Of these considerations, safety factors were found to be the largest variables in estimating fatigue lives because safety is affected by (1) constant life reduction, which multiplies total damage or reduces the number of cycles by a constant factor, and (2) statistical reduction, according to which allowable stress is reduced by a percentage based on the known degrees of variability of properties of materials.

When performing a system analysis or study, FATPLUS uses an online or preprogrammed spectrum, which is applied to a materials curve (a complex curve based on the more conservative of constant life reduction or statistical life reduction). Total damage and allowable life are determined from a combination of input from the user and cycles in the input spectrum. Because all users will not have access to corporate or private fatigue data, the developers of FATPLUS provided MIL-HNDBK-5 data on materials.

FATPLUS is therefore a superior program. Since release, this multifaceted program has proved itself strong and adaptable. FATPLUS can be expected to become used widely across private industry and government as users become more aware of all the program has to offer.

FATPLUS is written in FORTRAN for execution on PC-compatible computers.

This work was done by Thomas Minyard and James A. Babb formerly of Lockheed Electronics and Space Corporation for **Johnson Space Center**. *The software with complete documentation is available with software from James Babb, Johnson Engineering, telephone (281) 228-7710.*
MSC-22537

Mechanics

Hardware, Techniques, and Processes

Inflatable Wing Leading Edges for High Lift and Deicing

The incidence of stall accidents could be reduced.

John H. Glenn Research Center, Cleveland, Ohio

Computational simulations and wind-tunnel tests have demonstrated the feasibility of using inflatable boots on the leading edges of airplane wings, both as devices to increase lift and as pneumatic deicing actuators. Assuming success in further research and development, the first applications would likely occur as retrofits to single- and twin-engine airplanes in general aviation (GA). Later, corporate and commuter turboprop airplanes would be included. The eventual incorporation of these boots into new GA airplane designs would be even more desirable because the boots could be integrated with overall wing structures to provide laminar flow in cruise.

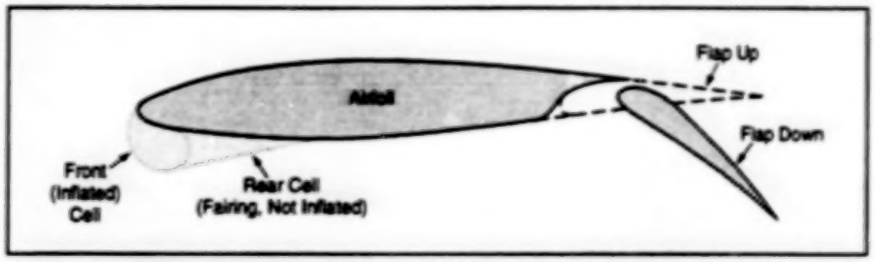

Figure 1. An Inflated Faired Boot installed on the leading edge of an airfoil can be used to increase lift and/or as a deicing actuator. A model with this configuration was used in wind-tunnel tests.

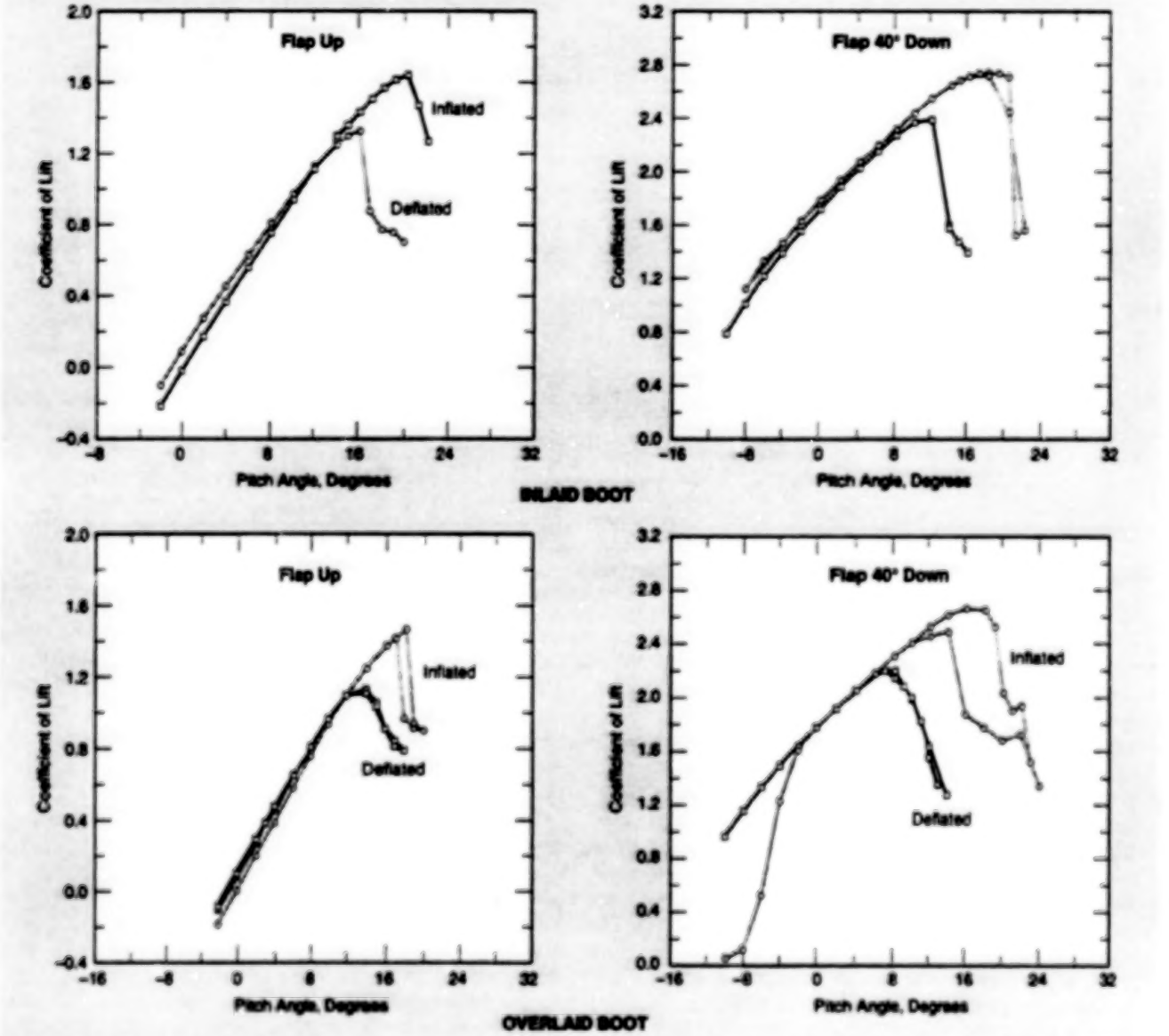

Figure 2. Maximum Coefficients of Lift and Angles of Stall Breaks were increased by inflation of boots, in both the flaps-up and flaps-down conditions.

The model used in the wind-tunnel tests and as the basis for the computational simulations was a standard airfoil (type 63-212 of the National Advisory Committee for Aeronautics) with a faired circular-arc boot installed on the leading

edge (see Figure 1). A boot of this type comprises front and rear cells. The front cell is shaped so that when it is inflated, its exposed leading-edge surface is nominally a portion of a circular cylinder. The rear cell serves as a fairing; it is vented to the atmosphere instead of inflated, and it is formed by attachment between a tangent line on the front cell and a line on the bottom surface of the airfoil.

Faired circular-arc boots for the wind-tunnel model were made of a standard deicing-boot material, and two different designs called "inlaid" and "overlaid" were tested. In the tests, inflation of both boots resulted in significant increases in the maximum coefficient of lift and the angle of the stall break (see Figure 2). Results of preliminary calculations based on the data from these tests suggest that it should be possible to achieve substantial increases in gross weight and reductions in stall speeds by use of faired circular-arc boots.

The use of inflatable leading-edge boots on GA airplanes would enable operation under known icing conditions and would thereby reduce the incidence of weather-related flight delays. High-lift features could be incorporated into deicing systems with very small increases in weight. Inflation of the boots for high lift would greatly extend angles of attack for maximum lift and would broaden the peaks of lift-vs.-angle-of-attack functions, thereby helping to prevent stall accidents.

This work was done by Kenneth G. Wernicke and Rodney K. Wernicke of Sky Technology Vehicle Design & Development Co. and Norbert A. Weisend, Jr., Consultant for **Glenn Research Center**. *Further information is contained in a TSP [see page 1].*

Inquiries concerning rights for the commercial use of this invention should be addressed to NASA Glenn Research Center, Commercial Technology Office, Attn: Tech Brief Patent Status, Mail Stop 7-3, 21000 Brookpark Road, Cleveland, Ohio 44135. Refer to LEW-16660.

Nonintrusive Flow-Measurement System

Flow is measured ultrasonically, from outside the pipe.

John F. Kennedy Space Center, Florida

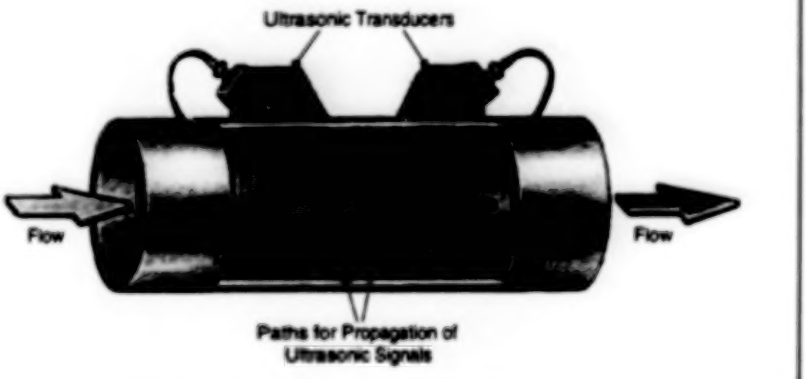

Transit Times of Ultrasonic Signals propagating upstream and downstream between the two transducers are measured. The flow velocity is calculated from the difference between the transit times.

A nonintrusive flow-measurement system based on ultrasonics has been developed to replace a system based on turbine flowmeters. A turbine flowmeter must be mounted in line with a pipe; this raises the possibility of leakage at the flowmeter/pipe joints, and the flowmeter unavoidably perturbs the flow. Moreover, a turbine flowmeter is vulnerable to mechanical malfunction and can be vulnerable to corrosion or clogging, depending on the nature of the fluid. In contrast, the ultrasonic flow-measurement system does not contain any rotating or sliding mechanisms that could fail, and does not involve any penetration of the pipe, so that the flow is not perturbed and there is no risk of leakage, clogging, or corrosion.

The nonintrusive ultrasonic flow-measurement system includes two ultrasonic transducers that are clamped on the outside of a pipe, at positions upstream and downstream from each other (see figure). Each transducer serves as both a transmitter and a receiver of ultrasound. The transducers are connected to electronic signal-generating and -processing circuits and a digital data-acquisition and -processing subsystem.

The basic measurement principle is straightforward: ultrasonic signals are transmitted in both directions between the transducers. The intervals between transmission and reception (transit times) are measured for signals propagating both upstream and downstream. When the fluid in the pipe is not flowing, the transit times in both directions are equal. When the fluid is flowing, the upstream transit time exceeds the downstream transit time. The difference between the transit times is proportional to the flow velocity and the volumetric flow rate. Accordingly, the direction and magnitude of flow are determined by use of digital signal-processing techniques and software that utilizes the known proportionality between transit times and flow velocity for the given fluid, physical conditions, and pipe size.

Unlike turbine flowmeters, the ultrasonic transducers can be easily and quickly relocated, and can be used to measure flow rates over a wide range without loss of accuracy at high or low rates. An additional advantage afforded by the ultrasonic system is the ability to detect partial or total loss of fluid from a pipe.

This technique was employed to accurately determine hypergol oxidizer and fuel loading during preflight space-shuttle operations. Benefits of ultrasonics include flexibility, cost-efficiency, reliability, and hazard-free hyperol operation. This technology also proved valuable in the determination of extremely low flow rates through the space-shuttle water-coolant-loop floodlight cold plate used for cooling the crew compartment.

This work was done by Rudy J. Werlink of **Kennedy Space Center** *and Ravi N. Margasahayam formerly of I-NET, Inc. Further information is contained in a TSP [see page 1].*

Inquiries concerning rights for the commercial use of this invention should be addressed to the Technology Programs and Commercialization Office, Kennedy Space Center, (407) 867-6373. Refer to KSC-11926.

Bushing-Mounted Drag Chain

A drag chain can be wrapped to a smaller radius than was previously possible.

Lyndon B. Johnson Space Center, Houston, Texas

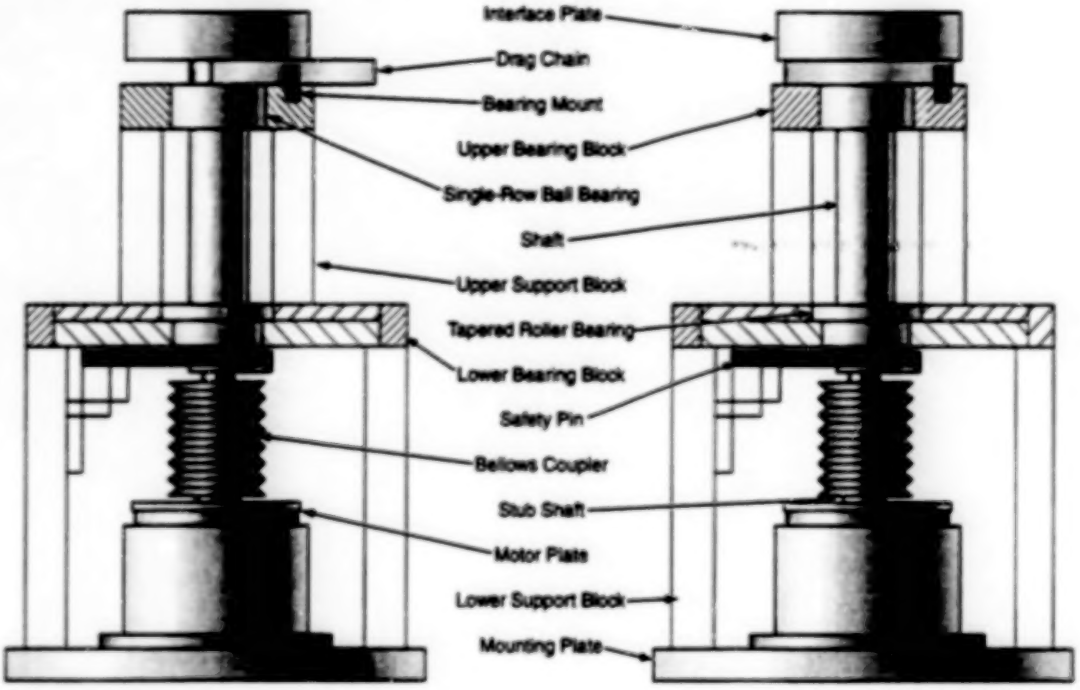

The **Chair-Base Mechanism** is connected to a drag chain via a bushing mount that reduces the amount of space needed to accommodate the drag chain.

The figure illustrates a chair-base mechanism with a bushing-mounted drag chain. The bushing-mount design provides for one end of the drag chain to be free to pivot; this provision makes it possible to wrap the drag chain to a radius smaller than that achievable in mechanisms previously designed for the same purpose. The utility of mechanisms like this one lies in applications in which rotation of machinery involves significant turning radii, so that bending of cables that run through drag chains involve relatively tight arcs.

The bushing-mounted drag chain contains cables and wires for actuating controls on a mechanical chair that can be rotated through 280° by use of the chair-base mechanism. In addition to being bushing-mounted, the drag chain is bearing-mounted on the upper bearing block; because of this, the bend radius of the chain varies with rotation of the chair in such a way as to maintain an overall compact system. This design feature reduces the amount of external floor space needed for a given length of drag chain and limits the overall length of the drag chain.

The chair-base mechanism with the bushing-mounted drag chain is in use at the Dexterous Robotics Laboratory at Johnson Space Center. The potential of the economical and efficient design of this mechanism has not yet been fully realized; future applications could occur in Hurco (or equivalent) drill presses, any similar rotating machinery in which drag chains are employed, and mechanisms for rotating gantry assemblies or other machinery.

This work was done by Myron A. Diftler of Lockheed Martin Corp. for **Johnson Space Center**. *No further documentation is available.*

MSC-22732

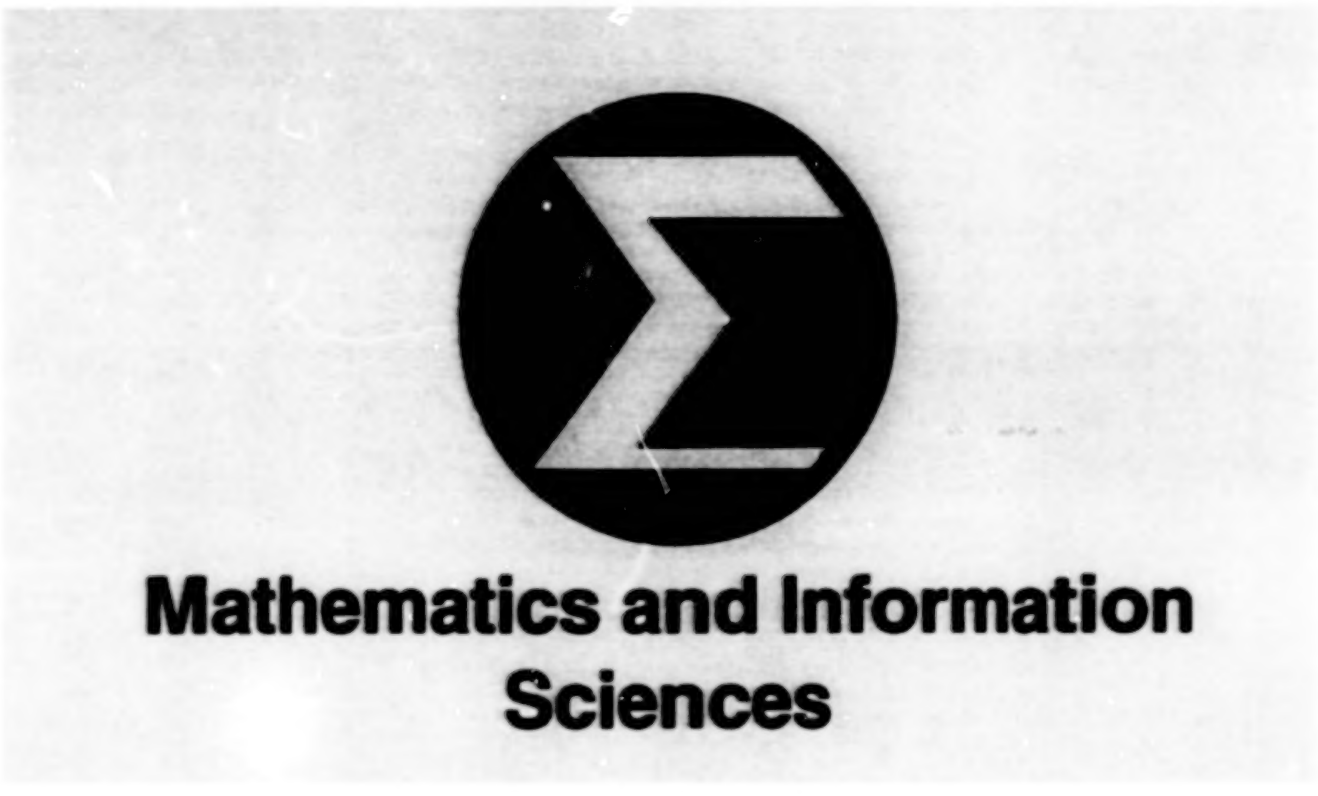

Mathematics and Information Sciences

Hardware, Techniques, and Processes

Algorithm for Rapid Acquisition of a PPM Optical Signal

Data frames can be synchronized with part of the synchronization sequence.

NASA's Jet Propulsion Laboratory, Pasadena, California

An algorithm for rapid acquisition of a pulse-position-modulation (PPM) optical data signal implements a pattern-matching technique for synchronization of receiver timing with the temporal boundaries of data frames. Synchronization is necessary because in PPM, information is conveyed by the time slot during which a pulse is detected. Fast acquisition of a signal depends on detection of pulses in noise, and on correct estimation of the times of detected pulses. To facilitate synchronization at the receiver, a transmitter periodically inserts a prescribed sequence of pulses — the synchronization sequence or word — into the transmitted data stream. Older PPM-signal-acquisition algorithms are based on correlations and depend on reception of the full synchronization word (128 bytes long in some applications). The present algorithm is more computationally efficient and is capable of achieving synchronization with part of the synchronization word — typically with as few as 2 to 6 bytes.

The algorithm involves, among other things, selective elimination of unlikely starting points for a sequence of received pulses detected in the presence of noise. It is assumed that the pulse-detection threshold of the receiver is set at a level that corresponds to a specified bit-error probability. The receiver is switched on at a random time, and a search for the synchronization sequence is started. The objective of the algorithm is to uniquely identify the temporal location of a received sub-sequence of the synchronization sequence.

Initially, the algorithm seeks all possible candidate sub-sequences that match a received 2-byte sequence. The process continues with the reception of additional bytes; the algorithm seeks matches with 3-byte sub-sequences, 4-byte sub-sequences, and so forth, until it eliminates all candidate sub-sequences that do not match and arrives at a single unique sub-sequence and thereby establishes the receiver timing relative to the entire synchronization sequence. The figure presents an example of this process in the case of a 32-byte synchronization sequence.

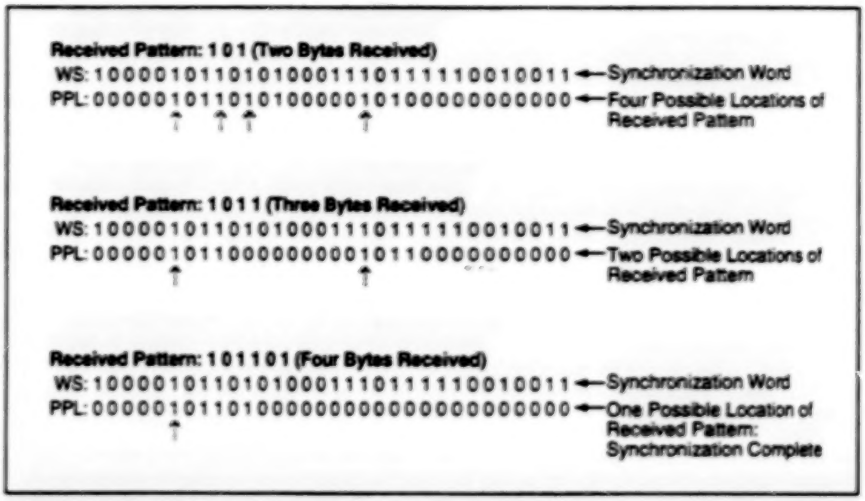

Received Byte Patterns are compared with sub-sequences of a 32-bit synchronization sequence. Matches with sub-sequences of increasing length are sought until the received pattern matches a unique sub-sequence.

When real data are interleaved between periodic transmissions of the synchronization sequence, data-bit patterns can sometimes be identical to sub-sequences of the synchronization sequence. Random bit flips caused by noise can also cause bit patterns other than the desired ones to alias as synchronization sub-sequences. To reduce the incidence of such errors, one can require confirmation in the form of additional received bytes beyond those needed to establish a unique synchronization sub-sequence; the additional bytes are said to constitute a confirmation sequence. The probability of false synchronization is inversely proportional to the length of the confirmation sequence.

The procedure for confirmation immediately follows the identification of a unique sub-sequence and determination of its starting time. The unique sub-sequence enables the algorithm to predict the arrival of the next pulse in the known synchronization sequence. If the next detected pulse arrives at the expected time, confirmation continues with the next pulse, and so on, for as many pulses as required for the confirmation sequence. If all predictions and observations have been found to match when the confirmation procedure has been completed, then synchronization is deemed to have been achieved and the temporal boundaries of data frames are calculated. If a mismatched pulse is detected during the confirmation procedure, then the algorithm resets.

This work was done by Payman Arabshahi, Tsun-Yee Yan, and Kourosh Rahnema of Caltech for **NASA's Jet Propulsion Laboratory**. *Further information is contained in a TSP [see page 1].*

NPO-20528

Post-Processing Satellite Image Data in Secondary Schools

Direct experience helps prepare children for participation in an increasingly technological world.

Goddard Space Flight Center, Greenbelt, Maryland

Never before have secondary schools been able to post-process raw satellite data, and now they can do it in real time. This is credited to advances in technology that have recently made the necessary equipment simple, inexpensive, powerful, and available enough for any school to fit into their technology-education curricula. This equipment couples ideally with the emerging utilization of the Internet in secondary schools.

Such precursors to the Internet as the direct satellite broadcasts called Advanced Picture Transmissions (APT) and Weather Facsimile (WeFax), were placed in schools over the past 15 years but never integrated into the curriculum. They provided Graphic Image Files (GIFs), i.e., snapshots of scenes

taken by satellites of the Earth below, by polar orbiting (NOAA) and geosynchronous (GOES) satellites, respectively. The operators of the satellites would produce these products on the ground and then uplink them to the same satellites for rebroadcast to the public. Users had no control over what images would be received nor could they enhance them to any notable extent. Recently, the Internet has supplanted this pathfinding service, by enabling the user to request such "canned" images on demand. Yet, due to the enormous amount of data in a single raw image (up to 385 MB), any attempt to access the raw data over the Internet must be severely constrained. Even high-speed connectivity is bogged down by the number of users all too quickly to use the Internet, for accessing anything larger than snapshots. This inherently limits the utility of the Internet services alone.

Now, innovations sponsored by GSFC have enabled us to bring raw, highest resolution, real-time data from the NOAA and GOES satellites to the secondary schools nationwide without compromise, at a price and complexity that they all can afford. This has required advancements in antenna design, a PC-based ingest and image processing system, and a curriculum that meets core learning goals and will be used by the teachers.

Standing Acoustical Wave (SAW) technology was applied to the low noise amplifier inside the antenna feed to better isolate the satellite downlink frequency and remove more of the background noise. This signal is then down-converted inside that feed to a lower frequency, before more noise can be picked up. The lower frequency preserves the signal-to-noise ratio along 300-ft (91-m) of inexpensive coaxial cable. A standard 10-ft (3-m) antenna used by homeowners for satellite TV, was adapted with this new feed, keeping the antenna costs to a minimum. Next, the expensive ($30k) radio receiver normally employed for access to multiple satellites, was replaced by a tailored version on a PC board that can sell for under $ 1,000. Likewise, the related external components were all designed onto PC boards, so that now the antenna feed plugs right into your PC, with no external components.

The software was rewritten to work on personal computers, which guarantees that the system will get faster, better, and cheaper every few months. At this writing, the entire system costs between $5.5k and $8.5k depending on the sophistication of the server computer and economy of scale for software licensing. Compare this to almost $200k for the first systems that NASA used to handle these functions.

The use of these new tools in secondary schools was introduced in 1996 when they still cost $25k. At that time, GSFC augmented the costs for two schools in Maryland and Pennsylvania, and they agreed to use the systems in technology-education programs.

Curricula were developed jointly over the next two years as the technologies and the application software improved and the price came down. Currently, schools in six states including the Pine Ridge Indian Reservation in South Dakota, are using these systems for academic credit. Students can use their Internet service to get ground truth images of wildfires, ocean currents, rain, snowfall, and the like. They can then locate the same time and place in their large data base of the raw satellite data, and custom enhance their images to match the ground truth. Having developed a suitable algorithm for rainfall where there is Doppler data and bucket measurements, they can now apply that algorithm to anywhere in the Western Hemisphere. Furthermore, using the continuous data from the geostationary satellites (GOES) they can apply their algorithms to the same scene every half hour or so and put it in motion. Now they can watch the rain/snow in motion or the wildfires move as they burn. Using emerging information technologies they can e-mail their customized film loops to other schools nationwide or beyond. The learning potential is enormous. They learn marketable technology skills in the areas of electronic access of information, post-processing of raw satellite image data, multimedia production, and both electronic and verbal communication skills, while doing really cool science projects. This critical part of the overall program has been a product of cooperation between the educators and NASA, as is essential if it is to be used for academic credits on a nationwide scale.

This work was done by Michael Comberiate of **Goddard Space Flight Center**, *George Isleib of GTI Electronics, and Shawn Terry of Aquila Systems. Further information is contained in a TSP [see page 1], or access the website: http://coolspace.gsfc.nasa.gov/*
GSC-14038

Further Developments in Web Interactive Training

Displays, simulations, and quizzes are customized for each trainee.

John F. Kennedy Space Center, Florida

Three innovative computer programs for training and testing personnel at Kennedy Space center have been developed under the aegis of the Web Interactive Training (WIT) project. The WIT project exploits the capabilities afforded by the Internet and by state-of-the-art multimedia data-presentation techniques. The World Wide Web is used to deliver training from server computers to client desktop computers on demand. Training can involve multimedia data of various types (text, audio, graphics, and animated video images). Training can be interactive, enabling trainees to tailor lessons to their individual needs; a trainee can select a lesson or segment any time, anywhere, and can repeat a segment as many times as necessary. Interactivity can also be exploited to provide for testing and recording of a trainee's progress.

One of the innovative programs provides a simulation of the International Organization for Standardization (ISO) 9000 certification process. By use of standard Hypertext Markup Language (HTML) pages and forms, the program creates an interactive system for ISO 9000 training. The client-side requirements for using the system are minimal; any popular Web-browser software can be used.

Each time the simulation is run, the events are slightly different. That is to say, the HTML pages are not static like ordinary Web pages; they are generated dynamically to create a more realistic representation of the simulated process.

The code on the server is highly object-oriented. The system can be expanded and new functionality can be added without disrupting the system. The user-interface part of the program is separate from the application part of the program; because of this architecture, new user interfaces can be created without modification of the main application code. Similarly, rules of a simulation can be changed without affecting the user interface.

Another of the innovative programs generates tests that are integral parts of a training course on techniques of nondestructive evaluation. The course is presented to each

trainee in modules. Each module includes (1) a video overview of a technique in action, (2) text and graphics that explain the theory and application, (3) an interactive simulation of an application of the technique (generated by the program described in the next paragraph), and (4) a quiz generated by random selection of questions from a data base of questions. Immediately after submitting answers, the trainee is presented with the test score, a brief explanation of the correct answers, and a link to the place in the course where the topic was covered. It is more difficult for a student to cheat because the program generates a different version of the quiz for each student and makes it impossible for any given student to take the same version of the quiz twice.

Still another innovative program is the one that generates the interactive simulations in the training modules. Each simulation is designed to give practice in one of a number of nondestructive testing processes: visual inspection, liquid-penetrant testing, magnetic-particle testing, eddy-current testing, leak testing, ultrasonic testing, or radiography. The simulations incorporate learning by example, repetition, and positive feedback. For example, in a simulation of the use of computed x-ray tomography of a solid cylinder, the student moves a scanner head along the cylinder while observing the scan on a simulated computer screen. Upon identifying a potential discontinuity, the trainee clicks on it; if the identification is correct, the simulation is immediately reset with the discontinuity scattered randomly to one or more different position(s). The trainee can repeat the simulation as many times as needed.

The advanced technology features of the WIT project contributed to the project winning a Gold Award in the 1997 multimedia and Internet Training Awards.

This work was done by Roger Wright, Thomas Brubaker, Angela Smibert, David Metcalf, and Tracy Bierman formerly of I-NET, Inc., for **Kennedy Space Center**. *Further information is contained in a TSP [see page 1], or visit the WIT Web site at http://wit.ksc.nasa.gov.*

Inquiries concerning rights for the commercial use of this invention should be addressed to the Technology Programs and Commercialization Office, Kennedy Space Center, (407) 867-6373, or for information regarding commercialization of this technology contact: Merrimac Interactive Media Corporation, 200 Willard, Suite 1A, Coca, FL, 32922, telephone: (407) 638-4118. Refer to KSC-11962.

Developmental Software for Exploiting Hyperspectral Imagery

Evolutionary computing techniques are used.

American GNC Corporation, Chatsworth, CA

A unique state-of-the-art process for exploiting hyperspectral satellite imagery, based on evolutionary computing methods, has been developed and a proof-of-concept demonstration has been conducted. This development is projected to lead to several important commercial products, including a fully integrated, high-payoff, user-friendly software package — the Integrated Hyperspectral Imagery Analysis Toolbox. This software would be capable of end-to-end processing of industrial and governmental hyperspectral satellite image data with extensions to several popular commercial software products like ENVI from Research Systems, Inc., and ESRI's ArcView Geographical Information System. The development of the end product will focus on accurate detection and identification of natural and artificial materials and objects, the use of large libraries of laboratory reference data, and ease of use. Potential commercial applications include assessment of crops (including estimation of crop yields), exploration for minerals and oil, planning of military missions and automated identification of military targets, urban planning, environmental assessment, and search-and-rescue operations.

The process effected by the proof-of-concept version of the software is the following: A spectral band signature is extracted from a hyperspectral satellite image and filtered to remove noise. It is then normalized to remove global gain differences. Next, an artificial neural network identifies those categories of objects and materials that correlate with the sensed data. The categories are expressed as orthonormal feature vectors derived from training signatures that were preprocessed in a manner similar to that of the sensed data. Finally, an evolutionary algorithm processes the output of the artificial neural network, detects the relevant materials, and estimates the amounts of the materials.

A computer program that performs an end-to-end computational simulation of the process has been developed. This program is capable of accepting real hyperspectral image data, performing the requisite processing on the data, and providing a graphical display of the results. The ENVI software, which provides a computational environment for rapid prototyping of other software, was used to facilitate the development of the simulation program. In the simulation, high performance in detecting and identifying materials in the terrain, including materials with spectrally mixed signatures, was demonstrated. Terrain-classification maps were generated, illustrating how signature variations can be handled, given terrain variations. Also demonstrated was an excellent capability to discriminate between strongly similar, but different, types of vegetation.

Further efforts are planned to accomplish the following:

- Development and execution of a data-collection plan (which would include the collection of ground-truth data) involving commercial and governmental sensors.
- Extension of public-domain atmospheric-compensation methods to include terrain topography.
- Updating of algorithms for improved performance against mixed spectral signatures, including signatures of unknown materials.

This work has been and will be undertaken by the **American GNC Corporation**, *9131 Mason Avenue, Chatsworth, CA 91311, an SBA 8(a) certified Small Disadvantaged Business concern, as part of a NASA Small Business Innovation Research (SBIR) project monitored by* **Stennis Space Center**. *The NASA SBIR Contract Number is NAS13-98208; Topic: 97-1 14.06; Topic Title: Measurement and Enhancement of Satellite Scientific Data Quality and Applicability. For further information, contact Dr. Ching-Fang Lin, American GNC Corporation, at tel: (818) 407-0092, fax: (818) 407-0093, or e-mail: cflin@americangnc.com.*

SBIR0007

Software for Processing Data in Particle-Image Velocimetry

This flexible, user-friendly program computes flow velocities from seed-particle images.

John H. Glenn Research Center, Cleveland, Ohio

PIVPROC is a computer program for processing data in particle-image velocimetry (PIV), which is a method of determining a flow velocity field from images of small seed particles that are entrained in the flow and that are illuminated by laser pulses at known intervals of time. PIVPROC creates an interactive computing environment for displaying and processing PIV image data. This environment includes a graphical user interface that provides user-friendly access to the image-data-processing capabilities of the program.

In PIV, a charge-coupled-device (CCD) camera records images that show the positions of the illuminated particles at two or more instants of time, then the image data are processed to extract velocities from the apparent displacements of the particles during the intervals between exposures. The processing involves one or more of three types of data-reduction techniques: autocorrelation, cross-correlation, and particle tracking. Autocorrelation is used to process double-exposure images, whereas cross-correlation and particle-tracking techniques are applied to pairs of single-exposure images.

In correlation processing, an image frame is divided into small subregions, each containing particle images. An auto- or cross-correlation operation is performed in each subregion, wherein the average displacement of the particles results in a displacement peak on a correlation plane. From the location of the displacement peak on the correlation plane and the time between laser pulses, the velocity in the subregion during that time can be computed. By thus processing the image over a regular grid of small subregions, one generates a velocity-vector map.

In particle tracking, displacements of individual particles are identified and used to compute velocities. In a combined correlation/particle-tracking operation, a correlation velocity-vector map is computed, then used as a guide for particle tracking.

The graphical work environment created by PIVPROC helps the user to perform autocorrelation, cross-correlation, and particle tracking operations on PIV image data. The raw PIV image data can be loaded and displayed on the computer screen. The image gain and threshold level can be adjusted by use dialog boxes. The correlation processing settings are also displayed in dialog boxes. Subregions wherein correlation processing is in progress are displayed in real time, along with the output correlation plane.

PIVPROC employs fuzzy logic for validating detections of correlation peaks and for determining correct particle pairings in particle-tracking operations; fuzzy logic enables the implementation of data-reduction algorithms that mimic or surpass the ability of a human operator to identify the correct particle pairings in the image data. PIVPROC supports the combined use of cross-correlation and particle tracking to obtain high-quality velocity data over a wide range of particle-seeding densities.

The velocity-vector maps generated by processing image data can be displayed, edited manually by use of the computer mouse, printed, and written to files. The data can also be interpolated; the program includes interpolation algorithms that enable the user to transform the spatially randomly sampled data from a particle-tracking operation onto a uniform grid of velocity vectors; the use of a uniform grid facilitates comparison of a velocity field determined by PIV with the corresponding velocity field determined by computational fluid dynamics.

PIVPROC runs in the Windows 95, Windows 98, and Windows NT operating systems. All of the data-processing and image-manipulation routines in PIVPROC are written in FORTRAN. The Microsoft Windows Application Programming Interface (API) functions are used to generate and service the interactive user environment.

This work was done by Mark P. Wernet of **Glenn Research Center**. *Further information is contained in a TSP [see page 1].*

LEW-16857

Expert System To Develop Job Standards

The Job Standards Development System is a user-friendly expert system that (1) helps users select an appropriate work measurement methodology to develop job standards (or the less formal job time estimates) and (2) leads the users through the steps necessary to use a work time estimating technique to develop job standards for long-duration, low-repetition work. The computer program comprises three parts, the first being a system-administration subprogram, in which an administrator sets values of parameters that are not changeable by a job standards developer. The second part is a subprogram that assists the job standards developer in the selection of an appropriate work measurement technique. The third part supports the application of a work time and resource requirement estimating technique that relies on domain expertise to describe human work, collects work time and resource requirement data from the domain expert, and computes a job standard. The program is expected to be useful for the management of organizations devoted to performing functions consisting of long-duration, low-repetition work. Illustrations of this type include facility and equipment maintenance and the knowledge work of service firms and federal, state, and local governments. The program is written for use with the Windows operating systems on IBM PC and compatible computers.

This work was done by Neal F. Schmeidler and John D'Avanzo of OMNI Engineering & Technology, Inc., for **Kennedy Space Center**.

In accordance with Public Law 96-517, the contractor has elected to retain title to this invention. Inquiries concerning rights for its commercial use should be addressed to

Neal Schmeidler
OMNI Engineering & Technology
7921 Branch Drive
Suite 530
McLean, VA 22102
Telephone No: (703) 827-8976
Web site: www.omni-engineering.com

Refer to KSC-12072, volume and number of this NASA Tech Briefs *issue, and the page number.*

Life Sciences

Hardware, Techniques, and Processes

Noninvasive Determination of Pressure in Cerebrospinal Fluid

Spinal taps would no longer be necessary.

NASA's Jet Propulsion Laboratory, Pasadena, California

A technique for noninvasive determination of the pressure in the cerebrospinal fluid (CSF) has been proposed. This technique would involve two main steps: First, an optical coherence tomographic scanner would be aimed into an eye and used to image the optical disk (see figure). Next, the resulting tomographic imagery would be digitized and processed to determine the thickness of the neural fiber layer, which thickness is known to increase with the CSF pressure.

Heretofore, the spinal tap has been the standard technique for measuring the CSF pressure (also known as the intracranial pressure or "ICP"). Spinal taps are painful, dangerous, and expensive. The proposed technique could make it unnecessary to perform spinal taps.

Papilledema — swelling of the optic-nerve axons in the optic disk — is known from previous studies to be associated with an increase in the intracranial pressure beyond the normal limit of approximately 14 mm of Hg (about 1.9 kPa). The neural fiber layer can swell to as much as 20 times its normal thickness within hours after the onset of elevated intracranial pressure.

Papilledema can be seen through an ophthalmoscope. Stereoscopic fundus photography and optic-nerve-head analysis also reveal aspects of papilledema. The common limitation of these previously developed optical techniques is that they depend on changes in surface topography. The proposed version of optical coherence tomography would measure the thickness of the neural fiber layer regardless of changes in surface topography, and should be capable of revealing swelling of axons earlier than do the previously developed optical techniques.

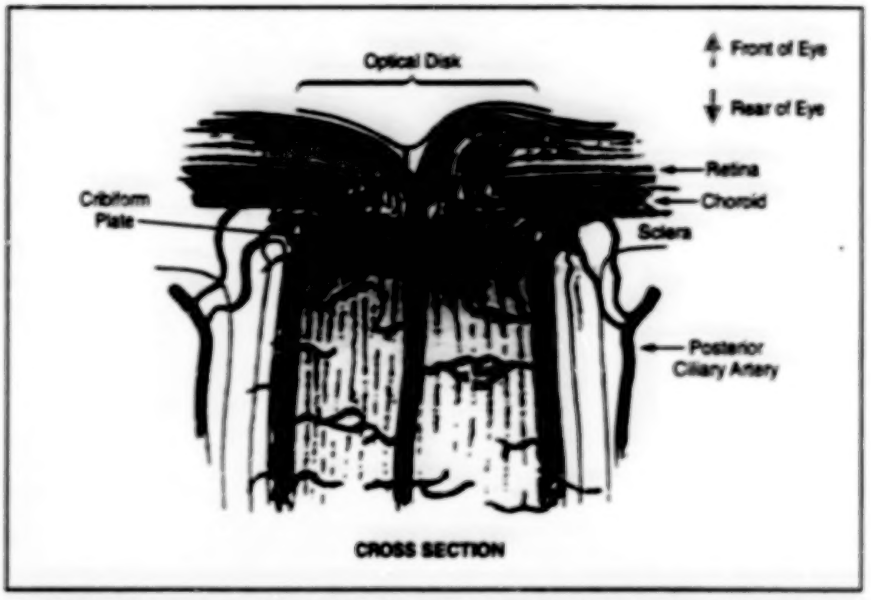

The Optic Disk (known popularly as the "blind spot") is the spot where the fibers of the optic nerve leave the eye. The thickness of the neural fiber layer in the optic disk increases with the intracranial pressure. According to the proposal, this thickness would be determined optically to obtain an indirect indication of the intracranial pressure.

By use of a previously constructed optical coherence tomographic scanner, it has been found that the thickness of the neural fiber layer in normal individuals varies by no more than 3 μm. This instrument has also been found capable of revealing early thinning of the neural fiber layer associated with glaucoma. Thus, it has been reasoned, it should be possible to use optical coherence tomography to measure early neural-fiber-layer swelling associated with intracranial hypertension. If the instrument could be modified to achieve a tenfold refinement of its resolution, then the instrument would be correspondingly more sensitive as an indicator of intracranial pressure. The modified instrument could be used in research on the sequence of events in papilledema because it could also provide information on deep and surface changes in the optic disk, flows of blood in veins and arteries, and shifts in the spectral reflectance of the optic disk.

This work was done by Mark S. Borchert and James L. Lambert of Caltech for **NASA's Jet Propulsion Laboratory.** *Further information is contained in a TSP [see page 1].*

NPO-20079

Improved Urine Preservative

This solution combines antibacterial and antioxidant properties.

Lyndon B. Johnson Space Center, Houston, Texas

An improved solution for preserving samples of urine has been formulated. This solution preserves a much broader spectrum of analytes in urine than do other urine-preservative solutions heretofore in use by NASA, and is safe for use by humans. When this solution is used, (1) refrigeration of urine samples is not necessary for preserving them and (2) the solution does not alter the pH values of the samples — two important considerations for collecting and storing urine samples in outer space. By eliminating the need to ship frozen samples, this preservative will enable the collection of urine samples — not only in outer space but also in terrestrial remote settings where it was previously not feasible.

Limits on overall available space and power aboard spacecraft include severe limits on available space for storing frozen biological fluids. Researchers at Johnson Space Center hoped to identify a way of preserving urine analytes at ambient temperature for long times to lessen the effects of these limits on biomedical research and monitoring of crew health. What they formulated is the present urine preservative, called "CPG," which is a solution that comprises equal parts of chlorhexidine gluconate and n-propyl gallate. CPG eliminates or reduces the primary causes of destruction of analytes in urine; these causes are bacterial contamination and oxidation. CPG does this without altering the pH of the urine. These characteristics make CPG an excellent candidate for use not only in outer space but also in the commercial

Analyte or Property	Duration of Stability (Compared to That of Unpreserved Urine Stored at –70° C)	
	Room Temperature	Room Temperature (Preserved by CPG)
Urea	28 days	12 months
Ammonia	Unstable	14 days
Calcium	Unstable	3 months
Creatinine	Unstable	Unstable
Sodium	7 months	5 months
Potassium	3 months	7 months
Chloride	4 months	4 months
Osmolality	Unstable	Unstable
3-Methylhistidine	6 months	3 months
Aldosterone	Unstable	14 days
Cortisol	Unstable	2 months
Cyclic Guanosine-5'-Monophosphate	Unstable	7 months
Melatonin	5 months	8 months
Total Nitrogen	2 months	3 months

Preliminary Data indicate that CPG preserves a number of urine analytes during prolonged storage at room temperature.

medical field on Earth.

Chlorhexidine gluconate is a water-soluble, bactericidal compound used commercially as a topical anti-infective agent. N-propyl gallate, a commercial food additive, is an antioxidant. The Food and Drug Administration has ruled that both compounds are safe for use by humans at the concentrations necessary to maintain the integrity of urine samples.

To make CPG, one first prepares 20-percent solutions of n-propyl gallate and chlorhexidine gluconate, then mixes these solutions in equal parts. The resulting CPG solution is placed into aliquot tubes to yield a final concentration of 0.4 milligram of CPG per milliliter of urine.

Researchers tested CPG with 17 urine analytes during 12 months, using two separate pooled samples. Unpreserved aliquots from each pool were stored at a temperature of –70 °C as baseline samples. Both preserved and unpreserved aliquots from each pool were also stored at room temperature. Analytes were measured on days 1, 14, and 28 for the first month and then once a month for the next 11 months. The table gives the results of this study. The bold text within the table indicates the instances in which CPG provided extended room-temperature stability.

This work was done by Scott Smith of **Johnson Space Center** *and Jeannie Nillen of Krug Life Sciences, Inc.*

This invention is owned by NASA, and a patent application has been filed. Inquiries concerning nonexclusive or exclusive license for its commercial development should be addressed to the Patent Council, Johnson Space Center, (281) 483-0837. Refer to MSC-22695.

Primers for Amplifying CMV DNA in Body Fluids and Tissue

A novel set of primers enables high-volume, rapid, inexpensive viral diagnostic testing.

Lyndon B. Johnson Space Center, Houston, Texas

A novel set of primers has been developed for use in a polymerase chain reaction (PCR) to amplify the deoxyribonucleic acid (DNA) of cytomegalovirus (CMV). The purpose of this development is to enable faster, more sensitive detection of CMV virus infecting body fluids and tissues.

Each year, in the United States, an estimated 40,000 infants are infected congenitally with CMV, which is a member of the herpesvirus family. CMV is the most common congenital viral infection in humans, and it is the leading infectious cause of mental retardation and nonhereditary sensorineural deafness. Studies show that CMV can survive from 2 to 48 hours in saliva and on environmental surfaces. Healthy adults usually experience unrecognized mild infections of this latent virus. For spaceflight crews, the pre-spaceflight quarantine period does not lessen the infectious-disease risks associated with latent viruses. Resulting viral illnesses can seriously affect the health of a crew.

The tissue-culture methods used heretofore for detecting CMV infections are labor-intensive, are subject to variability among technicians, lack sensitivity and specificity, and are time-consuming (taking 4 to 21 days in each case). The present PCR method with the novel primers overcomes these deficiencies of tissue-culture methods. The first primer — the sense strand, is a 21-base-pair oligonucleotide; the second primer — the antisense strand — is an 18-base-pair oligonucleotide. The use of these primers makes it possible to detect CMV infections directly from specimens of urine, saliva, blood, cerebrospinal fluid, and feces. These primers and the PCR method satisfy requirements with respect to preparation of specimens, sensitivity relative to traditional methods, and clinical significance of results. Applications also include detection of relapse of infection and testing the effectiveness of the antiviral therapy.

The development of this set of primers to amplify viral DNA by PCR offers a rapid, high-volume, and less expensive means (relative to tissue-culture methods) of viral diagnostic testing. Patients who have AIDS or cancer, transplant recipients, and others who are susceptible to CMV infections would receive the most benefit from this method of rapid detection.

This work was done by Duane L. Pierson of **Johnson Space Center** *and Raymond P. Stowe of KRUG Life Sciences, Inc. Further information is contained in a TSP [see page 1].*

Title to this invention has been waived under the provisions of the National Aeronautics and Space Act [42 U.S.C. 2457(f)], to KRUG Life Sciences, Inc. Inquiries concerning licenses for its commercial development should be addressed to

Raymond P. Stowe
KRUG Life Sciences, Inc.
1290 Hercules Drive
Suite 120
Houston, TX 77058
(281) 212-1200

Refer to MSC-22694, volume and number of this NASA Tech Briefs *issue, and the page number.*

END

02-18-00